NTNU – Trondheim
Norwegian University of
Science and Technology

Ice ridge keel size distributions

Analysis of ice ridge keel thickness from
Upward Looking Sonar data from the Fram
Strait using extreme value theory.

Synnøve Kvadsheim

Physics
Submission date: May 2014
Supervisor: Patrick Joseph Espy, IFY
Co-supervisor: Knut Høyland, BAT, NTNU

Norwegian University of Science and Technology
Department of Physics

Summary

The present thesis explored sea ice ridges in the Fram Strait from data collected at 79° N, 65° W in 2006/2007 by an Upward Looking Sonar instrument, IPS4, and used extreme value analysis to provide an estimate of how deep sea ice ridges could be in this area, and its return period. Ice in the Fram Strait originate from different regions in the Arctic Ocean and is therefore representative of the ice ridge distribution in the Arctic.

Ice ridges were identified using the Rayleigh method, choosing a threshold value of 2.5 m and a minimum draft value of 5 m.

The mean keel draft value was found to be 7.7 m. The shallowest keel observed had a draft of 5.0 m, while the deepest keel was 24.97 m deep. Extreme value analysis was performed on the data collected to find estimates of extreme values of ice ridge keel draft, and its 100-year return level. The shape parameter in the Generalized Pareto distribution was estimated to be close to zero, which qualified for a reduction to the Exponential distribution. The 100-year return level was estimated to be in the range of 37–45 m with the Generalized Pareto distribution and the Exponential distribution. The Weibull distribution was also used in the same analysis, but gave a much lower result with a 100-year return level of 29 m. The fraction of ice observed defined as ice ridges was 3%. The probability of encountering ice ridges deeper than 20 m was 0.15%, corresponding to previous results from similar analysis.

Sammendrag

Hoveddelen av denne master oppgaven var å utforske skrugarder i Framstredet fra data samlet inn ved 79° N, 65° V i løpet av 2006/2007, av en oppad pekende sonar kalt IPS4, og videre bruke ekstremverdi analyse til å estimere hvor dyp en skrugard kan bli i dette området, og dens tilhørende returperiode. Is i Framstredet stammer fra flere forskjellige deler av Arktis, og kan derfor sies å være representativt for hele regionen.

Skrugarder ble identifisert ved å bruke Rayleigs metode, med en terskelverdi på 2.5 m og en minimumverdi for skrugarder på 5 m.

Den gjennomsnittlige dybden på skrugardene var 7.7 m. Den grunneste av disse hadde en dybde på 5.0 m, mens den dypeste var 24.97 m dyp. Ekstremverdi analyse ble brukt på dataene for å estimere ekstremverdiene til skrugarddybden og dens tilhørende 100-års verdi. Formfaktoren til den generaliserte Pareto fordelingen lå rundt 0, og fordelingen kunne derfor bli redusert til en eksponential fordeling. Ut fra dette ble 100-års verdien estimert til å ligge i mellom 37 of 45 m. Weibull fordelingen ble også brukt til samme estimasjon, hvor resultatene ble en lavere 100-års verdi på 29 m. Fraksjonen av is undersøkt som ble definert som skrugarder var 3%. Sannsynligheten for skrugarder dypere enn 20 m ble estimert til å være 0.15%, som stemmet godt overens med tidligere studier.

Preface

Write your preface here...

Table of Contents

List of Tables

List of Figures

Chapter 1

Introduction

Increasing interest and activities in Arctic areas in the world require an increased knowledge of the sea ice dynamics in the given area. Sea ice ridges are often the most important ice features that can affect and damage platforms and pipelines in areas where a dynamic ice cover is present. The depth of ice ridges are therefore of great interest, particularly the extreme values of depth. Extreme value analysis is used to estimate the return levels of ice ridge depth values. Probabilistic extreme value theory deals with stochastic behavior of maximum and minimum values of independent, identically distributed random variables. In ice ridge depth analysis, this theory can be used in finding the extreme values that is possible in the area, with an associated return period.

Sea ice ridges are a form of mechanically deformed ice. They are linear features with a large mass of ice below the waterline, and a smaller mass of ice above the waterline. They form when relatively level ice sheets which has grown thermodynamically, move relative to each other causing mechanical failure and hence are deformed. Instead of sliding over each other, the ice sheets break, causing an ice rubble pileup, composed of rubble ice blocks arbitrarily piled together, which are then compressed together forming ridges. This breaking of the ice sheets or ice floes is caused by compression and shear from environmental forces. Of these the wind and sea current are the most important. The undersurface of sea ice is very variable, and the physical mechanisms that produce ice ridges and the extreme values of these may occur far from the area of interest. Ice in the central Arctic regions will use approximately one year to reach the Fram Strait (Hansen et al., 2013).

The Fram Strait is a dynamic area, located between Greenland and Svalbard, where ice fields are affected by the northbound West Spitsbergen Current and the southbound East Greenland Current. Ice are continuously being transported from the Arctic through the strait, giving the Fram Strait a unique position in that the drift of ice through the strait, is an indicator of the ice conditions in the Arctic. Sea ice in the central Arctic Ocean takes approximately one year to reach the Fram Strait (Hansen et al., 2013). A special characterization of the Fram Strait is a high frequency of ice ridges. According to Ekeberg et al.

(2012) there are observed approximately between 3000 and 11000 ice ridges each month in the Fram Strait.

Upward Looking Sonars have been used to measure ice thickness from below the water surface since the 1960s, first mounted on submarines, until bottom moored sonars started deployment in the late 1970s (Pilkington and Wright, 1991). These sensors take measurements of the ice draft every 2 seconds. Continuous sampling for a long period of time gives long time-series containing measurements of hundreds or thousands of individual ice ridges, depending on location of measurements and the time frame used.

The data used in this study were collected from September 2006 to September 2007 at $78°49'3.30''$ N, $6°26'48.12''$ W (mooring F14), in the Fram Strait. The instrument used for ice draft observations was an IPS4 instrument, located at approximately 58 m depth, with the local water depth of 281 m ((Ekeberg et al., 2012).

Chapter 2

About Ice

2.1 Ice Crystal Structure

Ice is the solid state of water, and is created when water reaches its freezing temperature at $0°$C. There are at least nine polymorph of solid water under different conditions of pressure and temperature, (Wadhams, 2000). Ice I is the only one that exists in significant quantities under normal physical conditions at earth's surface, (Wadhams, 2000). It consists of two hydrogen atoms and one oxygen atom, H_2O, covalently bonded with an angle of $105°$ (Notz, 2013). The oxygen atoms are concentrated to a series of parallel planes called basal planes, and are located perpendicular to the principal axis, called the c-axis of the structure. The hydrogen atoms in ice crystals follow the Bernal-Fowler rules (Marchenko, 2013):

1. The water molecule is preserved: two hydrogen atoms reside near each oxygen atom, and O-H distance is about 1 Angström.
2. Each lattice position is occupied by a water molecule which is tetrahedrally bonded to four nearest neighbors.
3. There is only one hydrogen per each oxygen-oxygen bond.
4. The hydrogen atoms are mobile, so that the first three conditions can be satisfied in any number of configurations.

The structure of ice (type I), **Fig. 2.1**, causes both physical and mechanical anisotropic properties. Taking fracture as an example; any fracture normal to the basal plane requires the breaking of minimum four bonds, while fracture along the basal plane requires only for two bonds to rupture. This again, causes ice to glide and cleave along the basal plane.

Because of the structure of the ice crystal, the preferred growth directions lie along the a- and b-axes rather than the c-axis, **Fig. 2.2**. It is easier to add new atoms to an existing

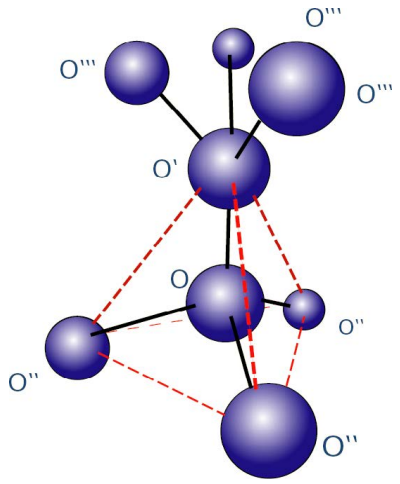

Figure 2.1: The structure of the ice lattice, type I

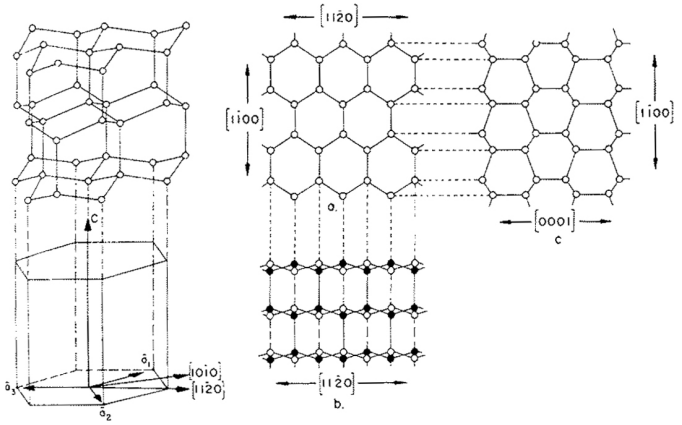

Figure 2.2: The hexagonal crystal structure of ice I

basal plane than to start a new plane of atoms. Examples of growth directions (list from Wadhams (2000)):

- The arms of snowflakes growing from vapour
- The arms of dendritic ice crystals growing on the surface of a newly-freezing sea or lake
- The preferred downward growth of sea ice crystals in a sheet)

2.2 Density and Freezing Point

The maximum density of a fresh water body is reached when the water reaches $3.98°C$ (Notz, 2013). Temperatures below this results in water becoming less dense and thus staying on the surface. This layer of colder water can then be rapidly cold down to the freezing temperature for fresh water at $0.0°C$. For fresh water it is thus possible for ice to form, even though the temperature of the underlaying water holds up to $4.0°C$.

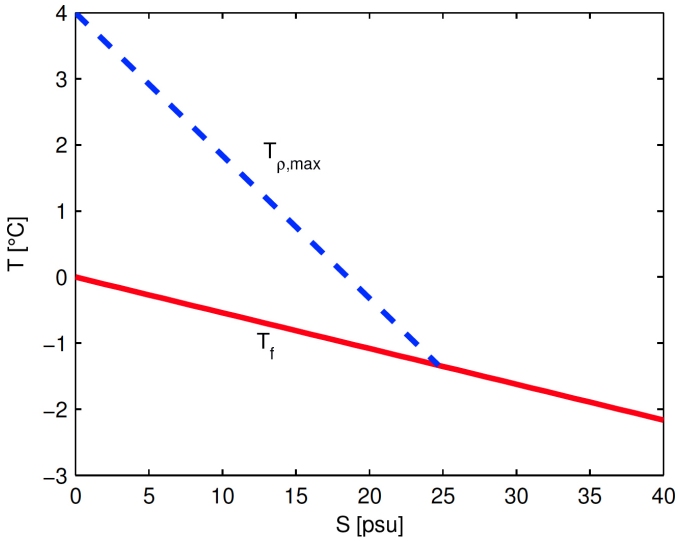

Figure 2.3: A temperature/salinity diagram, showing the freezing point of sea water and the temperature of maximum density as a function of salinity

The freezing temperature for sea ice is lower than the freezing temperature for fresh ice, and is a function of both salinity and pressure. The salt water in the world's ocean has a salinity of about 35 ppt (part per thousand weight fraction) (Høyland, 2012).

The addition of salt in the water lowers the temperature at where it will reach maximum density, as seen in the figure. When salinity exceeds $24,7$ psu (practical salinity units) the temperature of maximum density disappears and the water reaches the freezing temperature for sea water at $-1.8°C$, (Wadhams, 2000). The temperature/salinity dependency is shown in **Fig. 2.3**. The cooling of a water column by a cold atmosphere causes denser surface water and convection of the cooled water. In sea water the pycnocline creates a density jump which stops the convection from involving deeper levels of the sea. Thus only the surface layer down to the pycnocline needs to reach $-1.8°C$ for the water to start freezing. When ice forms it tries to expel the salt from the sea water, even though some salt is trapped during ice growth. Sea ice then consists of pure ice, gas, saltwater and, if the ice is cold enough, more water within the brine pockets freeze and expel solid salts (Høyland, 2012). The saltwater, or brine, is trapped in brine pockets which is then expelled through brine channels, causing old ice having lower salinity than fresh ice, see

Fig. 2.4. The salinity of first-year ice is about $3 - 8$ ppt, while old-ice has a salinity of $1 - 3$ ppt on average (Høyland, 2012). Sea ice is a two-phase multi-component material consisting of a solid phase with pure freshwater ice and a liquid phase with brine (Notz, 2013).

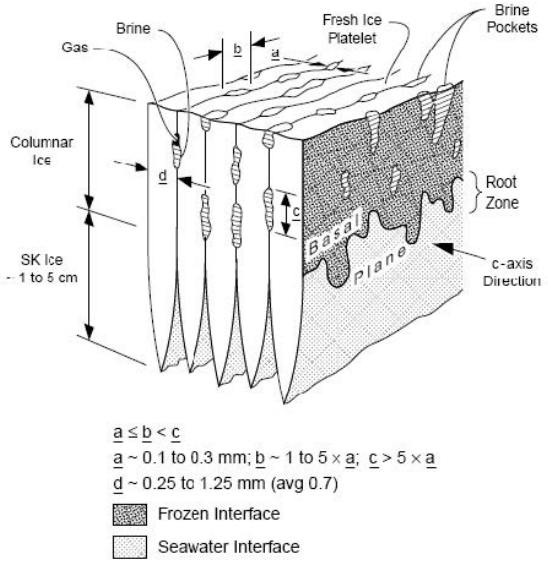

Figure 2.4: Sketch showing the ice structure with brine pockets and axis orientation

2.3 Ice Formation

As a cold atmosphere continually cools down the surface sea water to freezing temperature, small needle-like ice crystals form, frazil ice. These crystals have a diameter of about $3 - 4$ mm and because of lower density than the surrounding sea water, the frazil ice float to the surface to accumulate. The further growth is dependent on calm or rough conditions. An overview of the process is seen in **Fig. 2.5**. Figures **2.6**, **2.7** and **2.8** are examples of the different stages sea ice experience when freezing.

Two important properties about ice is that; 1) it is warm, that is it is at all times very close to its melting point, and 2) the ratio between the ice crystal size and the ice thickness is high. These properties cause ice to behave both elastically, visco-elastically and viscously (Høyland, 2012).

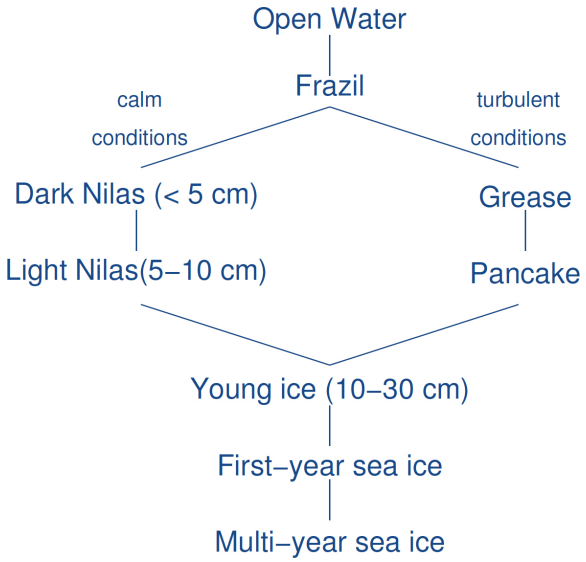

Figure 2.5: Diagram showing the evolution of the freezing of ice, from open water to multi-year ice, dependent on calm or turbulent conditions.

Figure 2.6: In calm conditions, the frazil ice crystals freeze together to form continuous thin ice sheets. When this sheet is transparent it is called dark nilas, but as the sheet grows thicker, the nilas become first grey, then white in appearance (light nilas).

Figure 2.7: In turbulent conditions, the frazil ice crystals are clumped together and form a thin, slushy layer resembling an oil slick, called grease ice.

Figure 2.8: When grease ice continuous to freeze, small coherent cakes of slush grow into disks. This is called pancake ice, because collisions between the disks forces frazil ice onto the edges of the disks, making them resemble pancakes when the water drains to leave raised rims of ice (Wadhams, 2000).

Chapter 3

About Ice Ridges

3.1 Morphology

Sea ice ridges are a form of mechanically deformed ice. They are linear features with a large mass of ice below the waterline, and a smaller mass of ice above the waterline. They form when relatively level ice sheets which has grown thermodynamically, move relative to each other causing mechanical failure and hence are deformed. Instead of sliding over each other, the ice sheets break, causing an ice rubble pileup, composed of rubble ice blocks arbitrarily piled together, which are then compressed together forming ridges. Sea ice ridges are also called pressure ridges due to this pressure during formation. This breaking of the ice sheets or ice floes is caused by compression and shear from environmental forces. Of these the wind and sea current are the most important.

Ice ridges are the thickest of ice formations, typically $5.0-30.0$ m, and over large areas the volume of these ridges may account for up to 50% of the total ice volume, (Leppäranta, 2011). They are several times thicker than the surrounding ice sheet, and are often found in the zone between land fast ice and drift ice (Tucker and Govoni, 1981).

An ice ridge consists of two main parts; ice blocks piled up on a level ice surface form the sail, the top part of the ridge, while submerged ice block form the keel, the lower part of the ridge. The spaces between blocks are filled with water and slush in the keel and snow and air in the sail. Because of hydrostatic equilibrium, the sail has a volume of about one tenth of the keel (Heinonen, 2004).

As ice blocks are pressed together due to a dynamic build-up, and freezing causes contact joints to form between the blocks, (Leppäranta et al., 1995). For the rubble to freeze together causing consolidation, only the water between the blocks need to freeze, (Leppäranta, 2011). This occurs at the waterline and a completely frozen layer called the consolidated layer forms. Latent heat is released from contact between ice blocks which warms the ice blocks in a fresh ridge, and is later conducted to the atmosphere giving

further consolidation downward inside the keel as the ridge ages. This freezing, or consolidation process progresses with time and a ridge are assumed to be fully consolidated if it survives the summer's melt. The ice blocks in the sail and the lower keel are loose or weakly frozen together, compared to the consolidated layer.

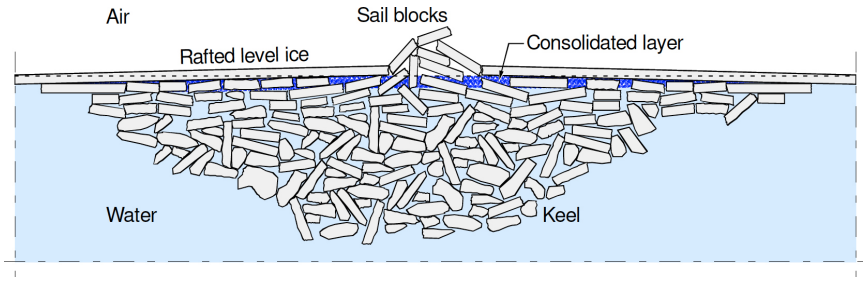

Figure 3.1: Sea ice ridge

Ice ridges are categorized by age; during its first winter the ice ridge is called a first-year ridge, while ridges that survive one or more summers are called second-year and multi-year ridges respectively. Ridges older than one year is also collectively called old ridges, (Ekeberg et al., 2013c).

The structure of an ice ridge undergoes continuously evolution during the season, with two important processes concerning the mechanical behavior of the ridge. These are the growth of the consolidated layer as water pockets freeze in temperatures below freezing, and the deterioration and smoothing of the surface rubble created by mechanical and thermal erosion from surrounding currents and climate. The most significant of these is the consolidation process. The internal structure of ice ridges is different from that of level ice, because the orientation of basal planes and c-axes has been reoriented in rubble ice (Heinonen, 2004). It has been found both by observation and by mathematical modeling that the thickness of the consolidated layer grows approximately 2 times faster than undeformed ice, (Leppäranta, 2011). The lower parts of the keel consist of loose ice blocks, and changes to the lower keel occur due to mechanical and thermal erosion as well as rearrangements in the block packing, (Leppäranta et al., 1995).

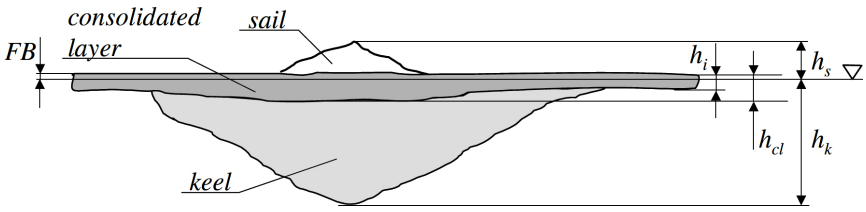

Figure 3.2: Sketch showing an average ice ridge with its components

According to Timco and Burden (1997) the overall shape off a first-year ridge can be

both variable and non-symmetrical; however they tend to be triangular in shape. During an experiment performed by Leppäranta et al. (1995) in 1991, during which the first three months of an ice ridge's life in the Bay of Bothnia, northern Baltic Sea, was investigated, it was found that the ridge structure experienced considerable evolution. It was found among other things that the external geometry of the ridge became smoother and that the cross-section of the ridge developed from triangular form toward trapezoidal form, reference figures **3.3** and **3.4**. The porosity of the ridge was found to decrease due to consolidation, with the mid-keel section at the minimum. When melting, the ice blocks in the lower keel were found to melt uniformly and the same as the overall ice volume decrease. Mechanical erosion of the keel was found to be of little significance.

Both first-year ridges and old ridges are very variable in shape and sizes, but they both have a general trend. Old or multi-year ridges tend to be larger than first-year ridges and are more rectangular in shape. Since old ridges have had time to freeze and grow due to continuously consolidation and pile up, they are usually heavier both in terms of frequencies and mean depths in comparison to first-year ridges, (Wadhams, 2012).

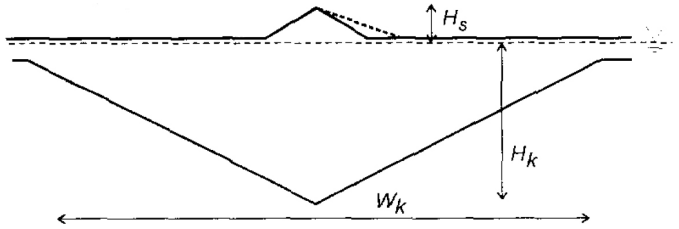

Figure 3.3: Sketch showing the shape of an average first-year ice ridge

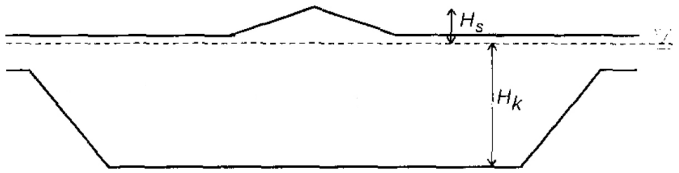

Figure 3.4: Sketch showing the shape of an average multi-year ice ridge

Shallow areas containing ice ridges where the sea depth is less than the keel depth, grounding of ridges occur, where they anchor to form fixed ice island, (Leppäranta, 2011). If properly influenced by its surroundings, the grounded ridge may start moving, scouring the ocean bottom, where the keel may penetrate deep into whatever bottom material (natural or artificial) that exist in the area.

In ice engineering, ice ridges are of deep concern because

- They are connected with the highest ice loads on structures within first-year ice fields
- They influence shipping conditions
- They scour the sea bottom
- They influence in-ice traffic conditions

(Leppäranta, 2011)

3.2 Ice Ridge Size

A physical limitation for ridge growth exists, (Leppäranta, 2011). If an ice ridge grows to a certain vertical size, an adjacent ice sheets is to week to penetrate into the ridge and instead breaks in front of it, producing lateral growth. The limiting size mainly depend on the thickness of the original ice sheet it was formed. The keel is normally about 4 times deeper than the height of the ridge sail, and also $2-3$ times wider, (Wadhams, 2000). Timco and Burden (1997) presented the following ratio for first-year ridges, where the cross-section was approximated using an ideal triangular shape.

$$\frac{h_{\mathrm{k}}}{h_{\mathrm{s}}} = 4.4 \tag{3.1}$$

Here h_k denotes keel depth and h_s sail height.

The much larger keel is a result of the fact that in a compressive deformation, it requires less energy to push ice block downwards against buoyancy than upwards against gravity. The largest ice ridge recorded was observed in the Beaufort Sea with a sail height of 12.0 m and a keel depth of 45.0 m, (Leppäranta, 2011).

In 2003 Amundrud et al. (2004) investigated a possible relationship between deformed ice and the adjacent level ice using ice draft observations from the Beaufort Sea, and found an empirical relationship between the keel draft,H, and the level ice draft, h.

$$H = 20h^{\frac{1}{2}} \tag{3.2}$$

The value of H represents the upper bound to the keel draft, the maximum size.

By estimating that a ridge keel has a triangular cross section with the width of the keel, w, equal to four times the draft of the keel, H (Timco and Burden, 1997), it is possible to calculate the extent of level ice needed to construct a ridge of maximum draft, by conserving the cross-sectional area (Amundrud et al., 2004). With f_{L} representing the length of

the floe and p its porosity,

$$f_{\mathrm{L}}h = \frac{1}{2}H(1-p) = 2H^2(1-p) \tag{3.3}$$

Substituting (3.2) into (3.3),

$$f_{\mathrm{L}}h = 800H(1-p) \tag{3.4}$$

From (3.4) it is seen that the minimum size of ice floe required to build a keel of maximum draft is 800 m, independent of the level ice draft. Continued ridging with an ice floe larger than 800 m, would increase only its width but not its draft.

By rearranging (3.3),

$$H = [\frac{f_{\mathrm{L}}}{2(1-p)}]^{\frac{1}{2}} \cdot h^{\frac{1}{2}} \tag{3.5}$$

From this Amundrud et al. (2004) proposed constraints on the maximum keel draft dependent on the restriction from (3.2) from the ice strength, and the restriction from (3.5) from the floe size. There is no unlimited supply of level ice in the Arctic available for ridging. The amount of ice and thus the amount of ice ridges are variable from season to season, with less ice recorded in the last years.

Ross et al. (2012) did the same analysis as Amundrud et al. (2004) using data obtained from the Fram Strait during 2008-2009, and found a similar relationship, but with a smaller scaling factor.

$$H = 17h^{\frac{1}{2}} \tag{3.6}$$

For an ice ridge to develop to its maximum size, several conditions have to be fulfilled. Firstly, sufficient adjacent level ice as raw material is needed. Secondly, it has to be sufficiently amounts of stress to cause structural failure of the ice. Thirdly, the critical stress must last long enough for the ridge to be built (Amundrud et al., 2004).

When the force that is needed to push an ice block beyond the top of a ridge exceeds the force that will collapse the level ice next to it is reached, the maximum height of the sail is reached (Hopkins, 1998). When this is reached, the level ice will fail and the fragments will contribute to either widening the existing ridge, or begin a new ridge.

Water depth may have an influence on maximum keel draft; shallow waters could function as a limiting factor. In deeper waters, there exists a finite probability that the maximum possible keel draft will pass by a specific location in a given time period (Ross et al., 2012).

Chapter 4

The Fram Strait

The Fram Strait is a narrow passage located between western Greenland and eastern Svalbard, **Fig. 4.1**, and is the only deep-water connection of the Arctic Ocean with the world's oceans, (Werner et al., 2013). It is the main export channel from the Arctic Ocean where sea ice is continuously exported with the Transpolar Drift (Ekeberg et al., 2013d). The Transpolar Drift is a major ocean current in the Arctic Ocean that carries sea ice and freshwater from Russian territories, across the North Pole towards Greenland, where it meets the East Greenland Current, that continues the transport of sea ice through the Fram Strait.

The sea ice outflow through the Fram Strait is a crucial component in the mass balance of the Arctic Ocean. It is estimated that roughly 10% of the total sea ice mass in the Arctic is exported through the strait every year, (Kwok et al., 2004). Because of this continuous drift of sea ice from the Arctic Ocean, the sea ice thickness in the Fram Strait is a natural indicator of the sea ice thickness in the Arctic. The ice in the strait consists of a mixture of first-year ice and old ice which originates from most parts of the Arctic Ocean (Ekeberg et al., 2013c). When and where the sea ice and the sea ice ridges in the Fram Strait are formed is unknown. The origin may vary from recent local formation to formation several years ago in distant locations (Ekeberg et al., 2013b). Concerning sea ice ridges, how a deep ridge deteriorates over time is unknown. But it is assumed that extreme sea ice ridges observed in the Fram Strait indicate the extremes in the Arctic Ocean.

The Fram Strait is an important part in the transport of heat to the Arctic and the freshening of the Nordic Seas through the sea ice export from the Arctic Ocean, (Werner et al., 2013). Warm and saline water flows into the Arctic basin through the West Spitsbergen Current (WSC) along the east side of the strait, a branch off the Norwegian Atlantic Current. The East Greenland Current (EGC) brings cold and low salinity water from the Arctic Ocean to the Northern Atlantic through the west of the strait, **Fig. 4.2**.

The ice flux through the strait is considered the largest component of the Greenland-Iceland-Norwegian Sea freshwater balance. It is the second largest freshwater flux on

Figure 4.1: A map showing the location of the Fram Strait

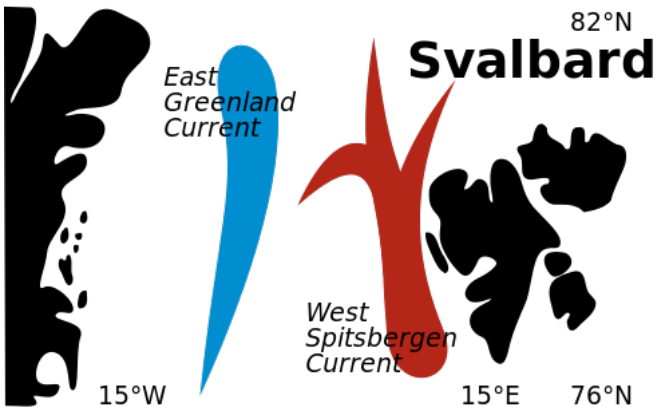

Figure 4.2: The northern flowing WSC (West Spitsbergen Current) and the southern flowing EGC (East Greenland Current)

Earth, after the Amazon River, and therefor affects the freshwater input in the North Atlantic greatly (Harder et al., 1998). The average time ice from different positions in the Arctic Ocean take to reach the Fram Strait varies from 1 year for ice north of Svalbard to 6 years for ice from the southern Beaufort Sea ((Vinje et al., 1998) /World Climate Research

Program(WCPR) 5, 1994).

Since 1990, The Norwegian Polar Institute has measured ice drafts along 79° N in the Fram Strait using bottom moored Upward Looking Sonars (ULS) (**?**).

Chapter 5

Measuring Ice Ridges

5.1 Instrumentation

5.1.1 Upward Looking Sonar

Several different technologies have been used to measure sea ice thickness from aircraft and satellites. Accurate estimation of the thickness using such technology is hindered by several factors, the most substantial being that $80\% - 90\%$ of the ice thickness lies below the waterline (Melling et al., 1995). In previous years, ice movement have been measured using satellites to track radio beacons that drift along with the ice field (Melling et al., 1995)(referenced Thorndike and Colony, 1982).

Upward Looking Sonar instruments, **Fig. 5.1**, have been used for several decades mounted on nuclear submarines to measure the ice thickness from below (Melling et al., 1995). But because of shallow water, the use of submarines over arctic continental shelves, have been problematic. In addition, issues of military security provided difficulties with routine ice monitoring. By mooring the sonars to the seabed, the measurements of sea ice can be executed all year and regardless of water depth (Melling et al., 1995). The natural drift of the ice pack continuously bring new ice into the field of measurement. However, the drift and the movement of the ice pack are highly variable, and the sampling is nonuniform. By supplementing the results from the moored ULS with an Acoustic Doppler Current Profiler (ADCP), which measures the ice drift speed, a conversion into a spatial series is possible (Ekeberg et al., 2013b). The combined data then provide a measure of the horizontal extent of the ice features. In the late 1970s and the early 1980s, Upward Looking Sonar prototype instruments were deployed in the Beaufort Sea (Pilkington and Wright, 1991).

Upward Looking Sonar instruments measure ice draft in areas containing sea ice, providing either time series (moored ULS) or spatial series (mounted to a submarine) of the draft.

The ice draft is determined by using a high temporal resolution and a spatial resolution. The temporal resolution use typically measurements at $1 - 2$ second intervals, and the spatial resolution with typically 0.05 m accuracy (Ross et al., 2012). The sonars conduct a continuous sampling over a long time period, and thus provide a long time series containing hundreds or thousands of individual ice keel features (depending on location and ice conditions). The spatial series are linear series representing the drafts of closely spaced points along imaginary linear tracks on the under surface of the ice pack. The ULS measures ice thickness by dispatching a sound pulse toward the ice pack at the surface, then measuring the time it takes to return to the sonar. The distance to the ice surface is then calculated using the speed of the sound above the ULS. Distance to the sea level is derived from pressure measurements at sea level and at the ULS. From this, ice thickness is calculated as the difference in distance between the sea level and the ice surface (Ekeberg et al., 2013c). The data from moored sonars are given as a sequence of ice draft values regularly spaced in time.

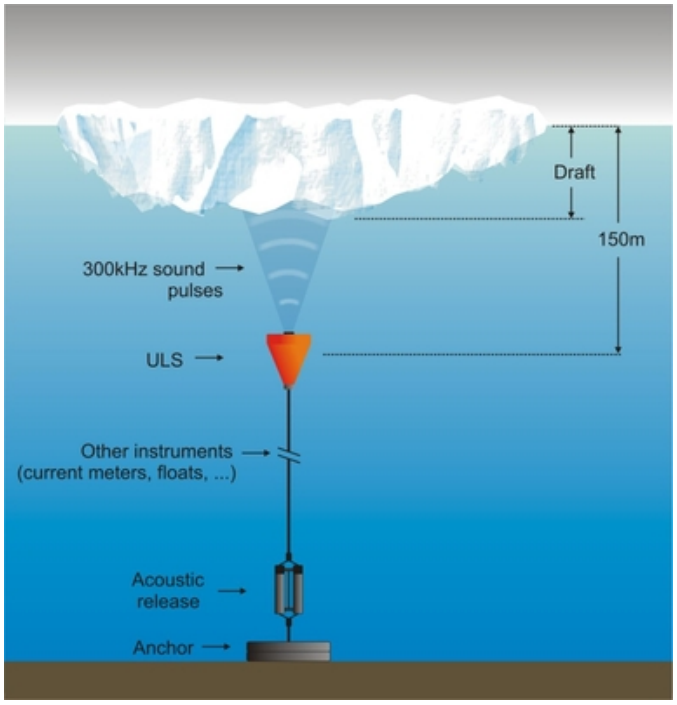

Figure 5.1: Upward Looking Sonar

5.1.2 Ice Profile Sonar

The Norwegian Polar Institute has since 1990, used upward looking sonars in the Fram Strait to measure the ice drafts along 79° N (**?**). In 2006 an ULS called IPS (Ice Profile Sonar of ASL Environment) was deployed. IPS measures the parameters pressure, range (time for echo to surface and back), and instrument tilt (Ekeberg et al., 2012). A sketch of an IPS instrument is shown in figure **5.2**.

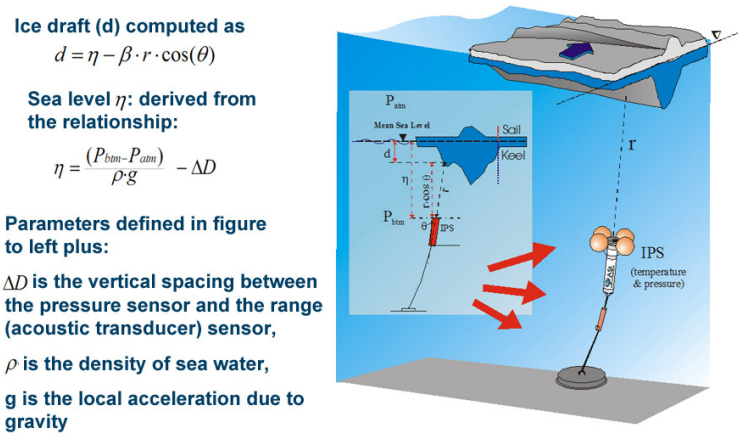

Figure 5.2: The ASL Ice Profiler (IPS) (asl, 2014)

The high sampling rate of the IPS ensures high resolution time series of the ice draft, and the detection of individual ice ridges in the ice pack. The IPS determines the time of short acoustic pulses from the instrument to a water column target and back to the instrument (Ross et al., 2012), with its beam directed to the zenith. With an ice pack above the sensor, a five-stage algorithm identifies the echo from the bottom of the ice pack (or from the sea surface). The algorithm then selects the echoes that are returned within a maximum range and beyond a minimum range, whose durations and amplitudes exceed certain chosen values. From these selected echoes, the one with greatest duration are chosen (Melling et al., 1995).

The IPS contains pendulum sensors used to measure the tilt of the sonar beam on two orthogonal axes which make it possible to calculate the zenith distance from echo range, a real-time clock, and a pressure-sensor (Melling et al., 1995). As the hydrostatic pressure at the IPS changes in response to tides, currents and storms, the pressure-sensor provides the actual depth of the IPS from the sea level. On average an IPS can view a spot nominally of $1 - 2$ m diameter at the surface with a depth of 50 m (Melling et al., 1995). But since the field of view depends on several external factors, it is not a fixed parameter. As mentioned, the sampling rate of the surface range is in seconds. Other variables like pressure are measured at intervals of minutes. The ice draft is measured every 2 seconds (Ekeberg et al., 2013c).

The IPS operate a narrow acoustic beam at 1.8° with a frequency at 420 kHz (asl, 2014), with a rapid sampling (up to 2 Hz) to obtain high resolution time series of the ice undersurface (Fissel et al., 2004). The beamwidth of 1.8° gives a footprint at the surface of 1.6 m. The beam hits the nearest point on the ice and reflects it back to the sensor. The range of the sensor is 175 m for ice and up to 225 m for water (asl, 2014). Combining the time series with the recorded hydrostatic pressure , regional-scale sea level atmospheric pressure and the sonar tilt, gives a time series representation of the ice draft above the sonar. The data recorded of pressure at the instrument is corrected for atmospheric pressure variations by utilizing downscaled ERA-40 reanalysis data provided by the Norwegian Meteorological Institute (Ekeberg et al., 2012). Eventual false subsurface targets and segments of draft records that may have been affected by waves are checked and flagged, while spikes and out-of-range data are replaced through linear interpolation (Ekeberg et al., 2012). These measurements enable conversions of the range measurements to the target draft through the relationship in equation (5.1), (Fissel et al., 2004):

$$d = \eta – \beta r \cos\theta \tag{5.1}$$

Here, d is the target draft, r the range to a target, θ the measured sonar tilt angle, and β is a time-dependent correction factor which accounts for changes in the mean sound speed in the upper water column. This correction factor is empirically found by identifying episodes of open water which, by definition, have zero draft (Ross et al., 2012). β is determined from the equation (5.2),

$$\beta = \frac{\eta}{r \cos\theta} \tag{5.2}$$

η represents the acoustic sensor depth and is established from the hydrostatic pressure measured by the sensor, P_{btm}, and the atmospheric pressure, P_{atm}, through equation (5.3);

$$\eta = \frac{P_{\text{atm}} - P_{\text{atm}}}{\rho g - \Delta D} \tag{5.3}$$

ΔD is the physical separation between the deployed acoustic sensor and the hydrostatic sensor in the vertical direction, ρ represent sea water density and g is the gravitational constant of $9.81 m/s^2$.

The time series can further be transformed to an equispaced distance interval, or spatial series, by integration with ice velocity measurements by an ADCP deployed co-deployed within 100 m of the IPS (Ross et al., 2012). ADCP stands for Acoustic Doppler Current Profiler, and is used to measure ice motion. It is a complex, microprocessor-controlled echo sounder that sends out an echo and then measures the Doppler shift of this echo

when it is returned (Melling et al., 1995).

A time series is sufficient in analysis of extreme ice draft (Ekeberg et al., 2013b), and data from an ADC is not used in this thesis.

5.1.3 Uncertainty

The process of calibration, measuring accurately at a certain point, and sampling includes several uncertainties. In statistical properties these are related to the number of independent observations along a draft profile (Melling et al., 1995). Because the IPS is dependent on the motion of the ice pack to provide new targets, the speed at which the ice pack moves can influence the results. If the speed of the ice pack between measurements exceeds the $1 - 2$ m field of view of the sonar, the ice profile will be under sampled. Small-scale features may be misinterpreted as larger features and aliasing occur. A very low drift speed may generate large quantities of unnecessary data. Small changes in IPS depth occur due to meteorological effects (wind, pressure etc.) (Melling et al., 1995).

The sonar must be placed deep enough to avoid impact or disturbances from the overlying ice pack (e.g. ice ridges or icebergs). In too deep water, where long mooring lines are necessary to position the sonar close enough to the ice surface; changing currents can cause significant displacements of the sonar, both vertical and horizontal.

5.2 Ice Ridge Keel Identification

5.2.1 Smoothing

The more a data set is smoothed, the fewer single points are found in the data set (Ekeberg et al., 2013a). By smoothing the ice draft data, fewer ice ridges are identified in the analysis. However, by smoothing the data, one avoids local minima within an ice ridge being mistaken as the end of the ridge, and a single ridge is hence not divided into several ridges. This leads to fewer ice ridges after the smoothing method is applied.

A running average filter was used in this study, with a window size of 10 seconds (5 points) (Ekeberg et al., 2013b), before the Rayleigh method was used, to avoid one ridge being identified as several due to local minima. The window size of 10 s corresponds to a horizontal distance with an average value of 2.1 m, which is close to the footprint of the instrument at 1.6 m (Ekeberg et al., 2013c).

5.2.2 The Rayleigh Criterion

In most studies, ice ridges are identified by using the Rayleigh criterion (Ekeberg et al., 2012). The Rayleigh criterion is used in optical physics as a way to determine when two

light sources are distinguishable from each other. It was defined by Lord Rayleigh in the 19th century, who proposed this limiting condition of resolution; when the central maximum of one image falls on the first minimum of another image, the images are said to be just resolved (Jewett and Serway, 2008). This criterion is possible to extend to identifying ice ridges, by defining the end points of an ice ridge keel, as it has been done in several studies; Obert and Brown (2011), Ekeberg et al. (2012), Wadhams and Horne (1980).

The Rayleigh criterion makes it possible to define a ridge as an ice feature that returns to some proportion of the keel's maximum depth at its beginning and its end. The ridge end is identified even if the surrounding ice is thicker than a chosen threshold value but not part of the ridge itself (Obert and Brown, 2011).

To define the extent of an independent ridge, the criterion determined by Wadhams and Horne (1980) is used;

the through on either side of a ridge's crest, which is the point of maximum keel draft, must descend at least to the midpoint towards the local ice surface. Wadhams and Horne (1980) defined an arbitrary threshold value of 2.5 m, which is still a common choice of threshold value. The threshold value is the distance from the water surface to the level ice surface, in other words; the level ice thickness subtracted the free-board (Ekeberg et al., 2012). By defining a threshold value, rafted or thickened ice which is not defined as ice ridges, is excluded. The value of 2.5 m originates from a time when most of the ice was multi-year ice and hence thicker than today. A value if 1.5 m is a more accurate value presently. But 2.5 m is still chosen for comparison and compatibility with data obtained (Wadhams, 2012).

The data is scanned until a draft record exceeds the chosen threshold value. The Rayleigh criterion then acknowledge this as the current start of an individual ridge, and the data are further scanned, continuously updating the maximum draft value, until the end of the particular ridge is reached. The end of a ridge is defined if the draft record is either less than the threshold value, or if it is less than the adaptive draft threshold and the slope has reversed (Ross et al., 2012). When the end of the ridge is defined, the start of the ridge is defined by searching backwards from the current start using the same criteria (Ross et al., 2012). After the scanning and identification of all the ridges are completed, ice features that overlap are combined to form a single ridge, and ridges found with only one record is removed.

Assuming that the data records move from left to right according to figure **5.3**, the Rayleigh method uses the parameters α, β and δ to determine if R1 and R2 are one independent ridge, or two separate ridges. α represents the distance from the chosen threshold value to the maximum observed draft value (the keel crest), β is the distance from the keel crest to the current draft record, when moving from left to right in figure **5.3**, and δ represents the maximum observed draft after identified local minimum (Ekeberg et al., 2012).

According to figure **5.3**, if $\beta < 0.5\alpha$, R1 and R2 are defined as one ridge with edges

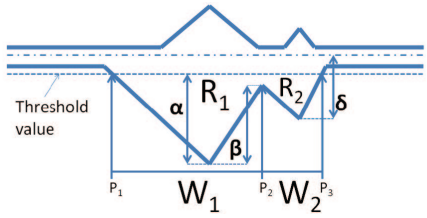

Figure 5.3: Definition of the values used in the Rayleigh ridge identification method, (Ekeberg et al., 2012)

P1 and P2.

If $\beta > 0.5\alpha$ and the following condition is fulfilled,

$\delta > 2 \cdot (\alpha - \beta) + h_{\text{thres}}$

R1 and R2 are defined as two separate ice ridges (Ekeberg et al., 2012). h_{thres} defines the threshold value.

In addition to a threshold value, a minimum draft is defined to avoid including minor ice features lying just below the chosen level ice value (Wadhams and Horne, 1980).

5.2.3 The Cutoff Method

The Cutoff method identifies an ice keel by an increase and a succeeding decrease in the ice thickness above a specified threshold value (Pilkington and Wright, 1991). By this definition, the ridge in figure **5.3** would be defined as one ridge with width $W_1 + W_2$, and with a maximum depth of $\alpha + h_{\text{thres}}$ (Ekeberg et al., 2012).

Ekeberg et al. (2012) compared the two methods of ice ridge identification, and discovered that the Rayleigh method identified more ridges than the Cutoff method. The Cutoff method will only detect the ridge with the deepest draft, if the ice thickness between consecutive ridges crosses the chosen threshold value. By increasing the threshold value when using the Rayleigh method, it will increase the likelihood of false identification of large ridges (Ekeberg et al., 2012).

In this study,the Rayleigh method was used with a threshold value of 2.5 m and a minimum draft value of 5 m. The minimum draft value of 5 m make certain that mechanically grown ice generally is defined as ice ridges (Ekeberg et al., 2013d). There may be large amounts of ridged ice below this draft value; however, ice beyond 5 m of thickness does not grow thermodynamically (Hansen et al., 2013). Ice deeper than 5 meters is then known to be formed dynamically and not thermodynamically.

Chapter 6

Statistics

6.1 Classic Extreme Value Theory

Extreme value theory originated due to the need for astronomers to evaluate outlying observations of distant objects in the universe, and determine whether to reject them or include them in their analysis (Kotz and Nadarajah, 2000). Extreme value analysis is used to study and quantify the stochastic behavior of any process at unusually large – or small- levels. In particular, this type of analysis requires estimation of the probability of events from a given ordered sample that are more extreme than observed. In classical data analysis these extremes are often labeled outliers and are ignored or smoothed out when analyzing the average value of a data set. In order to estimate events or behavior that do not happen often, extreme value theory is applied. Extreme value theory focuses on the statistical behavior of

$$M_{\mathrm{n}} = max\{X_1, ..., X_{\mathrm{n}}\} \tag{6.1}$$

where $X_1, \ldots, X_{\mathrm{n}}$ is a sequence of independent random variables with a common distribution function F (Coles, 2001). The X_{i} represents values of a process measured on a regular time scale; hence M_{n} represents the maximum value of this process over n time units.

It is possible in theory to calculate the distribution of M_{n} for all values of n:

$$\begin{aligned} Pr\{M_{\mathrm{n}} \leq z\} &= Pr\{X_1 \leq z_1, ..., X_{\mathrm{n}} \leq z\} \\ &= Pr\{X_1 \leq z\} \times ... \times Pr\{X_{\mathrm{n}} \leq z\} \\ &= \{F(z)\}^{\mathrm{n}} \end{aligned} \tag{6.2}$$

But the distribution function of M_{n}, F, is unknown, and estimates by approximate models are required.

6.2 Extreme Value Distributions

The Extremal types theorem states that if sequences of constants given as $\{a_{\mathrm{n}} > 0\}$ and $\{b_{\mathrm{n}}\}$ exists such that

$$Pr\{\frac{M_{\mathrm{n}} - b_{\mathrm{n}}}{a_{\mathrm{n}}} \leq z\} \rightarrow G(z), \quad n \rightarrow \infty \tag{6.3}$$

and G is a non-degenerate distribution function (Coles, 2001), then G belongs to one of the three extreme value distributions;

$$G(z) = \mathrm{e}^{-\mathrm{e}^{[-\frac{z-b}{a}]}}, \qquad -\infty < z < \infty \tag{6.4a}$$

$$G(z) = \begin{cases} 0 & z \leq b \\ \mathrm{e}^{-(\frac{z-b}{a})^{-\alpha}} & z > b \end{cases} \tag{6.4b}$$

$$G(z) = \begin{cases} \mathrm{e}^{-[-(\frac{z-b}{a})^{\alpha}]} & z < b \\ 1 & z \geq b \end{cases} \tag{6.4c}$$

for parameters $a > 0$, b and $\alpha > 0$. These distribution families are called the Gumbel family, the Fréchet family and the Weibull family respectively (Coles, 2001).

M_{n} can be stabilized by a normalized variable $M*$ as follows,

$$M* = \frac{M_{\mathrm{n}} - b_{\mathrm{n}}}{a_{\mathrm{n}}} \tag{6.5}$$

The Extremal types theorem then implies that $M*$ then has a limiting distribution that must be one of the three families; Gumbel, Fréchet or Weibull.

The three families of extreme value distributions can be combined into a single family of models called the Generalized Extreme Value (GEV) family of distribution, as seen in (6.6),

$$G(z) = \mathrm{e}^{-[1+\xi(\frac{z-\mu}{\sigma})]^{-\frac{1}{\xi}}} \tag{6.6}$$

This equation is defined for parameters $-\infty < \mu < \infty, \sigma > 0, -\infty < \xi < \infty$, defined on $\{z : 1 + \xi\frac{z-\mu}{\sigma} > 0\}$. Here μ is a location parameter, σ a scale parameter and ξ a shape parameter (Coles, 2001).

$\xi > 0 \rightarrow$ Fréchet, with $\alpha = \frac{1}{\xi}$
$\xi < 0 \rightarrow$ Weibull, with $\alpha = -\frac{1}{\xi}$
$\xi = 0 \rightarrow$ Gumbel

By assuming that

$$Pr\{\frac{M_{\mathrm{n}} - b_{\mathrm{n}}}{a_{\mathrm{n}}} \leq z\} \approx G(z) \tag{6.7}$$

for large n, it is possible to approximate the distribution of M_{n}:

$$\begin{aligned} Pr\{M_{\mathrm{n}} \leq z\} &\approx G\{\frac{z - b_{\mathrm{n}}}{a_{\mathrm{n}}}\} \\ &= G*(z) \end{aligned} \tag{6.8}$$

where $G*$ is a member of the GEV family.

Traditional GEV models use the concept of block maxima, which describe how data are blocked into sequences of a specific period length, n, which the GEV distribution can be fitted. The most common choice for a time period is the length of a year, in which case, n represents the number of observations in a year and the block maxima are then the annual maxima (Coles, 2001). Quantiles are points or specific elements that are taken at regular intervals of a distribution dividing the values of the distribution into equal proportions. The simplest of these are obtained by dividing data into two equal halves and you get the quantile called median; by dividing the data into four equal parts you get quartiles; by dividing into five parts you get quintiles, etc (Hagen, 2010). Quantiles allow for probability models to be expressed on the scale of data according to Coles (2001), which means that the relationship of GEV models to its parameters, are most easily found using the quantile expression in equation (6.9).

$$z_{\mathrm{p}} = \begin{cases} \mu - \frac{\sigma}{\xi}[1 - y_{\mathrm{p}}^{-\xi}] & \text{for } \xi \neq 0 \\ \mu - \sigma \log y_{\mathrm{p}} & \text{for } \xi = 0 \end{cases} \tag{6.9}$$

where $y_{\mathrm{p}} = -\log 1 - p$, $G(z_{\mathrm{p}}) = 1 - p$ and p is defined as the probability that z_{p} is exceeded by the block maxima in any particular year (Coles, 2001). z_{p} is also known as the return level with $1/p$ being the return period; the level z_{p} is expected to be exceeded on average once every $1/p$ years (Coles, 2001).

6.2.1 Maximum Likelihood Estimation

The maximum likelihood estimation is a general method of estimating an unknown parameter, θ_0, within a known family of distribution F. It is based on maximizing the likelihood of the observed data (Castillo et al., 2005). Values within $\theta \in \Theta$ defines a model in F that associate different probabilities to the observed data. The probability of the observed data as a function of θ is called the likelihood function (Coles, 2001). The principle of the maximum likelihood estimation is to come up with the model with greatest likelihood, which will be the model with the highest probability of the observed data. $f(x; \theta_0)$ is a given probability density function with $x_1, \ldots, x_{\mathrm{n}}$ independent realizations of a random variable (Coles, 2001), we can define the likelihood function as

$$L(\theta) = \prod_{i=1}^{n} f(x_{\mathrm{i}}; \theta) \tag{6.10}$$

The most likely parameter estimates are found by taking the logarithms of (6.10), and get the log-likelihood function as shown in equation (6.11).

$$l(\theta) = \log L(\theta) = \sum_{i=1}^{n} \log f(x_{\mathrm{i}}; \theta) \tag{6.11}$$

6.2.2 Confidence Intervals

A confidence interval is an interval estimate that contains a high probability for every possible value of an unknown parameter x (Bertsekas and Tsitsiklis, 2002). We get a range of values it is possible to be "confident" of that the true parameter value lies within (Coles, 2001). The frequency of which the observed interval has the parameter included is determined by the confidence coefficient. The definition of a confidence interval is as follows (Dougherty, 1990):

If (θ_1, θ_2) is an interval estimator, where

$$P(\theta_1 < \theta < \theta_2) = 1 - \alpha$$

and we define $\acute{\theta_1}$ and $\acute{\theta_2}$ as estimates that results from a set of sample values, the interval $(\acute{\theta_1}, \acute{\theta_2})$ is called a $(1–\alpha) \cdot 100\%$ confidence interval.

$1–\alpha$ is the confidence coefficient. $\acute{\theta_1}$ are called the lower confidence limit, $\acute{\theta_2}$ are called the upper confidence limit.

6.3 Chebyshev's Inequality

Markov's and Chebyshev's inequalities are important theorems in statistics, as they allow for derivations of bounds of probabilities when only the mean value and the variance of a probability distribution are known (Ross, 2009). (Markov's inequality uses the mean value, while Chebyshev's inequality also uses the variance of the distribution).

Markov's inequality theorem (Ross, 2009):

X is defined as a random variable that only takes nonnegative values. For any value $a > 0$;

$$\begin{aligned} E[X] &= \int_0^\infty x f(x) \mathrm{d}x \\ &= \int_0^a x f(x) \mathrm{d}x + \int_a^\infty x f(x) \mathrm{d}x \\ &\geq \int_a^\infty x f(x) \mathrm{d}x \\ &\geq \int a f(x) \mathrm{d}x \\ &= a \int_a^\infty f(x) \mathrm{d}x \\ &= a P\{X \geq a\} \end{aligned}$$

which can be written as

$$P\{X \geq a\} \leq \frac{E[X]}{a} \tag{6.12}$$

As a corollary from Markov's inequality we get Chebyshev's inequality;

X is defined as a random variable with mean μ and variance σ^2. For any value $k > 0$;

$$P\{\mid X - \mu \mid \geq k\} \leq \frac{\sigma^2}{k^2} \tag{6.13}$$

Proof of Chebyshev's inequality:

$(X - \mu)^2$ is a nonnegative random variable. Because of this, we can use Markov's inequality and define $a = k^2$ to obtain

$$P\{(X-\mu)^2 \geq k^2\} \leq \frac{E[(X-\mu)^2]}{k^2} \tag{6.14}$$

We have that $(X-\mu) \geq k^2$ if and only if $\mid X-\mu \mid \geq k$. This means that equation (6.14) is equivalent to

$$P\{\mid X-\mu \mid \geq k\} \leq \frac{E[(X-\mu)^2]}{k^2} = \frac{\sigma^2}{k^2} \tag{6.15}$$

Another way of expressing Chebyshev's inequality is by replacing k by $k\sigma$ in (6.14) above. We then get

$$P\{\mid X-\mu \mid > k\sigma\} \leq \frac{1}{k^2} \tag{6.16}$$

From this equation it is seen that the probability of a random variable to differ from its mean by more than k standard deviations is constrained by $1/k^2$. Chebyshev's inequality states that a significant number of the values in a probability distribution are close to its mean; less than or equal to $1/k^2$ values differ from its mean by more than k standard deviations.

$$P\{\mid X-\mu \mid < k\sigma\} \geq 1 - \frac{1}{k^2} \tag{6.17}$$

6.4 Exponential Distribution

The exponential distribution, also called the negative exponential distribution, is a probability distribution used to model events that occur continuously at a constant average rate, λ. The probability density function (PDF) of the exponential distribution is (Castillo et al., 2005)

$$f(x) = \begin{cases} \lambda \mathrm{e}^{-\lambda x} & \text{if } x \geq 0 \\ 0 & \text{if } x < 0 \end{cases} \tag{6.18}$$

and a cumulative distribution function (CDF)

$$F(x) = \begin{cases} 0 & \text{if } x < 0 \\ 1 - \mathrm{e}^{-\lambda x} & \text{if } x \geq 0 \end{cases} \tag{6.19}$$

The exponential distribution is a continuous memoryless random distribution, which means that if the random variable X is associated with e.g lifetime, the probability of X exceeding a given time b is independent of the of time origin of a (Castillo et al., 2005).

$$Pr(X > a + b \mid X > a) = Pr(X > b) \tag{6.20}$$

6.4.1 Extreme Value Prediction

It has been found experimentally that the distribution of keel drafts along a linear track in an ice field obey an exponential distribution (Wadhams, 1983) according to equation (6.20);

$$n(h)dh = B\mathrm{e}^{-bh}\mathrm{d}h, \quad h > h_0 \tag{6.21}$$

Here, $n(h)$, represents the number of keels per km of track per meter of draft increment, and the values of B and b are derived in terms of experimentally observed mean keel draft (h_m), the mean number of keels per unit distance (n_k) and the threshold value h_thres (Wadhams, 2012).

$$b = \frac{1}{h_\mathrm{m} - h_\mathrm{thres}} \tag{6.22}$$

$$B = n_\mathrm{k} b \mathrm{e}^{bh_\mathrm{thres}} \tag{6.23}$$

By using (6.21) it is possible to estimate the total number of keels each year that passes a given point with drafts exceeding a chosen value D,

$$N_\mathrm{D} = \int_\mathrm{D}^\infty n(h)\mathrm{d}h = Ln_\mathrm{k}\mathrm{e}^{\frac{h_\mathrm{thres}-D}{h_\mathrm{m}-h_\mathrm{thres}}} \tag{6.24}$$

where L is the distance in km drifted per year by the ice field over the given point.

Return Level

By using equation (6.24), it is possible to find the return period expressed in years, T_D for a keel of depth D or greater;

$$T_{\mathrm{D}} = \frac{1}{N_{\mathrm{D}}} \tag{6.25}$$

Where N_{D} represents the total number of ridge keels passing by a given point per year. If the return period is specified, equations (6.24) and (6.25) above can be used to calculate the keel depth at which the required return period occurs (Wadhams, 2012):

$$D = h_0 + (h_{\mathrm{m}} - h_0) \ln T_{\mathrm{D}} L n_{\mathrm{k}} \tag{6.26}$$

6.5 Weibull Probability Distribution

The probability density function (PDF) describes the relative likelihood of a continuous random variable having a given value. The cumulative distribution function (CDF) is the probability of a random variable X with a given probability distribution having a value that is less than or equal to x;

$$F(x) = P\{X \leq x\} \tag{6.27}$$

The CDF of X can be expressed in form of the PDF of X;

$$F(x) = P\{X \leq x\} = \int_{-\infty}^{x} f(t)\mathrm{d}t \tag{6.28}$$

The PDF of a three-parameter Weibull distribution is given by equation (6.29), (Castillo et al., 2005). This is the most general expression of the Weibull PDF.

$$f(x) = \frac{\beta}{\delta} \mathrm{e}^{-(\frac{x-\lambda}{\delta})^{\beta}} (\frac{x-\lambda}{\delta})^{\beta-1}, \quad x > \lambda \tag{6.29}$$

The CDF of a three-parameter Weibull variable is given by equation (6.30), (Castillo et al., 2005).

$$F(x) = 1 - \mathrm{e}^{-(\frac{x-\lambda}{\delta})^{\beta}}, \quad x \geq \lambda \tag{6.30}$$

To linearize the cumulative Weibull distribution, the natural logarithm is used.

$$1 - F(x) = \mathrm{e}^{-(\frac{x-\lambda}{\delta})^{\beta}} \tag{6.31}$$

$$\ln 1 - F(x) = \ln \mathrm{e}^{-(\frac{x-\lambda}{\delta})^{\beta}} = -(\frac{x-\lambda}{\delta})^{\beta} \tag{6.32}$$

$$\ln \ln 1 - F(x) = \beta \ln x - \lambda - \beta \ln \delta \tag{6.33}$$

The straight line in the equation is then define by

$$y = ax + b$$

where
$y = \ln \ln 1 - F(x)$
$a = \beta$
$x = \ln x - \lambda$

6.5.1 Extreme Value Prediction

The three-parameter Weibull distribution is often used in extreme value analysis (Ross et al., 2012). The General Extreme Value Distribution for the three-parameter Weibull distribution is given as

$$L(x) = \begin{cases} 0 & \text{if } x < \lambda \\ 1 - \mathrm{e}^{-(\frac{x-\lambda}{\delta})^{\beta}} & \text{otherwise} \end{cases} \tag{6.34}$$

The parameters in the equations above represent a shape parameter, β, a scale parameter, δ, and a location parameter, λ. This expression is the same as the CDF of the three-parameter Weibull distribution, and written in terms of the exceedance probability, $E(x)$, you get an expression for maximum values greater than value x (Ross et al., 2012);

$$E(x) = 1 - \mathrm{e}^{-(\frac{x-\mu}{a})^{b}} \tag{6.35}$$

Here, a represents the scale parameter, b the shape parameter and μ the location parameter. In equation (6.35) the location parameter optimizes the fit to empirical cumulative probabilities for individual keel draft values (Ross et al., 2012). By finding values for these parameters allows for the computation of D_{100}, the 100-year return period for keel depth. In practical terms, if N number of keels is included in the development of empirical cumulative probability distributions for S sites and Y years, equation (6.36) gives the 100-year return period in terms of exceedance probability $E(x)$.

$$E(D_{100}) = \frac{\sum_{j=1}^{S} Y_{\mathrm{j}}}{100N} \tag{6.36}$$

$E(D_\mathrm{i}$ gives the empirical values for exceedance as a function of lesser draft values, with D_i the ith keel draft value, and i the index of this draft value (Ross et al., 2012);

$$E(D_\mathrm{i}) = 1 - \frac{i}{N+1} \tag{6.37}$$

6.6 Generalized Pareto Distribution

If one block of data contains more extreme events than another, it may better to use another method of evaluating extreme values than block maxima (Coles, 2001). The approach is then to use a threshold model, also known as a Peak-over-Threshold (POT) model, in which an extreme event is defined as one that exceeds a given threshold value. The generalized Pareto distribution (GPD) is a family of continuous probability distributions.

$X_1, X_2, \ldots$ are defined as independent and identically distributed random variables, having marginal distribution function F. Extreme events are defined as those of the X_i that exceeded some high threshold u. Utilizing these conditions, it follows that a description of the stochastic behavior of extreme events is given by the conditional probability Coles (2001),

$$Pr\{X > u + y \mid X > u\} = \frac{1 - F(u+y)}{1 - F(u)}, \quad y > 0 \tag{6.38}$$

The generalized Pareto distribution theorem states as follows:

$X_1, X_2, \ldots$ is a sequence of independent random variables with common distribution function F that satisfies (6.6), and let

$$M_\mathrm{n} = max\{X_1, ..., X_\mathrm{n}\} \tag{6.39}$$

for large n

$$Pr\{M_\mathrm{n} \leq z\} \approx G(z) \tag{6.40}$$

where

$$G(z) = \mathrm{e}^{-[1+\xi(\frac{1}{z}-\mu_\sigma)]^{-\frac{1}{\xi}}\}} \tag{6.41}$$

for some $\mu, \sigma > 0$ and ξ. Then the distribution function of $(X - u)$, conditional on $X > u$, for large enough u, is approximately

$$H(y) = 1 - (1 + \frac{\xi y}{\tilde{\sigma}})^{\frac{1}{\xi}} \tag{6.42}$$

defined on $\{y : y > 0 \text{ and } (1 + \frac{\xi y}{\tilde{\sigma}}) > 0\}$, where

$$\tilde{\sigma} = \sigma + \xi(u - \mu) \tag{6.43}$$

The distribution family in (6.42) is called the Generalized Pareto Family (Coles, 2001), with ξ the shape parameter and σ the scale parameter. $F(X)$ is defined as the common distribution function, $H(y)$ is the distribution function of $(X - u)$, and u is the threshold value. The shape parameter ξ is the dominant parameter in determining the qualitative behaviour of the GPD, as it is for the GEV distribution. If $\xi < 0$, the distribution of excesses has an upper limit of $u = \tilde{\sigma}/\xi$. If $\xi > 0$, the distribution has no upper limit (Coles, 2001). If $\xi \to 0$, from (6.42) we get

$$H(y) = 1 - \mathrm{e}^{-\frac{y}{\tilde{\sigma}}}, \quad y > 0 \tag{6.44}$$

which is correspondent to an exponential distribution with parameter $1/\tilde{\sigma}$ (Coles, 2001).

6.6.1 Threshold

The threshold value should be as low as possible according to Coles (2001), although the value choice is not an easy one. A too low threshold value may violate the asymptotic basis of the model; while a too high threshold value will not generate enough excesses with witch the model can be estimated. There are two methods of selecting a reasonable threshold value for the generalized Pareto distribution (Coles, 2001). The first method is based on the mean value of the distribution;

$$E(Y) = \frac{\sigma}{1 - \xi} \tag{6.45}$$

for $\xi < 1$. If $\xi \geq 1$, the mean is infinite (Coles, 2001). We define u_0 as the threshold of a series of measurements, $X_1, \ldots, X_{\mathrm{n}}$.

$$E(X - u_0 \mid X > u_0) = \frac{\sigma_{u_0}}{1 - \xi} \tag{6.46}$$

for $\xi < 0$. σ_{u_0} is the scale parameter corresponding to the values exceeding u_0. The GPD is valid for all thresholds $u > u_0$. For $u > u_0$, and using the results in equation (6.43),

$$E(X - u_0 \mid X > U_0) = \frac{\sigma_u}{1 - \xi} \quad = \frac{\sigma_{u_0} + \xi(u - u_0)}{1 - \xi} \tag{6.47}$$

For $u > u_0$, $E(X–u \mid X > u)$ is the mean value of the values that exceeds the threshold value u, and the sample mean of the values exceeding u provides an empirical estimate (Coles, 2001). According to equation (6.47), these estimates are expected to change linearly with u (Coles, 2001), that leads to the following procedure:

The locus of points

$$\{(u, \frac{1}{n_u} \sum_{i=1}^{n_u} (x_{(i)} - u) : u < x_{max}\} \tag{6.48}$$

where $x_1, ..., x_{n_u}$ consists of n_u observations that exceeds u. x_{max} is called the residual life plot (Coles, 2001). above the threshold, u_0, the mean residual life plot is approximately linear in u (Coles, 2001).

The second procedure of choosing an appropriate threshold value is a method where the model is estimated at a range of thresholds. By the generalized Pareto distribution theorem, if the GPD is a logical model for exceedance of a given threshold value u_0, then exceedance of a higher threshold, u, should also follow a GPD. The shape parameter are identical for the two distributions. From equation (6.43):

$$\sigma_u = \sigma_{u_0} + \xi(u - u_0) \tag{6.49}$$

6.6.2 Return Level

It is more beneficial to use quantiles or return levels rather than individual parameter values when interpreting extreme value models (Coles, 2001). A generalized Pareto distribution with parameters σ and ξ, are used for modeling exceedance of a threshold value u by a variable X, that is for $x > u$,

$$Pr\{X > x \mid X > u\} = [1 + \xi(\frac{x-u}{\sigma})]^{-\frac{1}{\xi}} \tag{6.50}$$

$\Rightarrow$

$$Pr\{X > x\} = \zeta_{\mathrm{u}}[1 + \xi(\frac{x-u}{\sigma})]^{-\frac{1}{\xi}} \tag{6.51}$$

where $\zeta_{\mathrm{u}} = Pr\{X > x\}$. The level x_{m} that is exceeded once every m observations are on average:

$$\zeta_{\mathrm{u}}[1 + \xi(\frac{x_{\mathrm{m}}-u}{\sigma})]^{-\frac{1}{\xi}} = \frac{1}{m} \tag{6.52}$$

$\Rightarrow$

$$x_{\mathrm{m}} = u + \frac{\sigma}{\xi}[(m\zeta_{\mathrm{u}})^{\xi} - 1] \tag{6.53}$$

for $x_{\mathrm{m}} > u$ and $\xi \neq 0$. For $\xi = 0$ we get

$$x_{\mathrm{m}} = u + \sigma \log m\zeta_{\mathrm{u}} \tag{6.54}$$

for $x_{\mathrm{m}} > u$ (Coles, 2001). x_{m} is here the m observation return level. By defining a number of observations per year, npy, this corresponds to x_{m}, where $m = N \cdot npy$, N being the return period in years. We get the N-year return level as

$$z_{\mathrm{N}} = u + \frac{\sigma}{\xi}[(N \cdot npy \cdot \zeta_{\mathrm{u}})^{\xi} - 1], \quad \text{for } \xi \neq 0 \tag{6.55}$$

$$z_{\mathrm{N}} = u + \sigma \log N \cdot npy \cdot \zeta_{\mathrm{u}}, \quad \text{for } \xi = 0 \tag{6.56}$$

Chapter 7

Results

A minimum keel draft value of 5 m was chosen in the analysis. This means, that all ice features, including ridges, with a draft below 5 m are not defined as ice ridges and hence not included in the analysis. The fraction of ice observed defined as ice ridges was 0.0299, approximately 3%. The mean value of keel draft was 7.7085 m, the minimum value 5.004 m and the maximum value 24.976 m. The median was 6.9850 m. The mean keel width was found to be 63.0508 m, the minimum value at 6.3565 m and maximum value of 1969.3 m. A relative correlation between measured keel width and keel area was found in figure **7.1**.

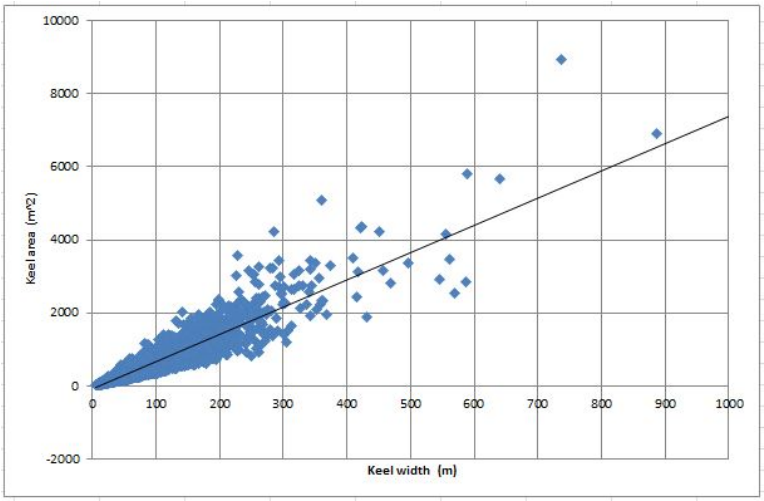

Figure 7.1: A correlation plot of ice ridge keel width and ice ridge keel area observed.

The smoothed data got a lower maximum draft value then the unsmoothed data, a slight increase in mean keel draft as well as a reduced number of ice ridges. The decrease in keel

draft per ridge was 2–5.5%. This resulted from the running average smoothing method used on the ice ridge data.

7.1 Chebyshev's inequality

Chebyshev's inequality states that at least $1–1/k^2$ of the data from a sample must fall within k standard deviations from the mean. The standard deviation is a measure of the deviation of a data set from its mean (Castillo et al., 2005).

Variance :

$$\sigma^2 = E[(X - \mu)^2]$$

Standard Deviation:

$$\sqrt{\sigma^2}$$

The value of standard deviation and variance of the keel draft, were found from calculations, and utilized in the Chebyshev's inequality formula. The variance was calculated to be

$$\sigma^2 = 6.3282,$$

and the standard deviation

$$\sigma = 2.5156.$$

For different threshold values we get **Table. 7.1**, that shows the probability of encountering keel draft of different values, according to Chebyshev's inequality theorem.

Threshold value u (m)	**Probability**
10	0.06328
15	0.02812
18	0.01953
20	0.01582
22	0.01307
24	0.01083
26	0.00936
30	0.00731

Table 7.1: Threshold value vs Probability

It is obvious that the probability of encountering large keel drafts decrease with increasing threshold values. There is a higher probability of observing ice ridges with smaller keel drafts than with larger keel drafts. The extremely deep ice ridges become increasingly rare as the keel draft increases. As u increases, the probability decreases, as

seen in **Fig. 7.2**.

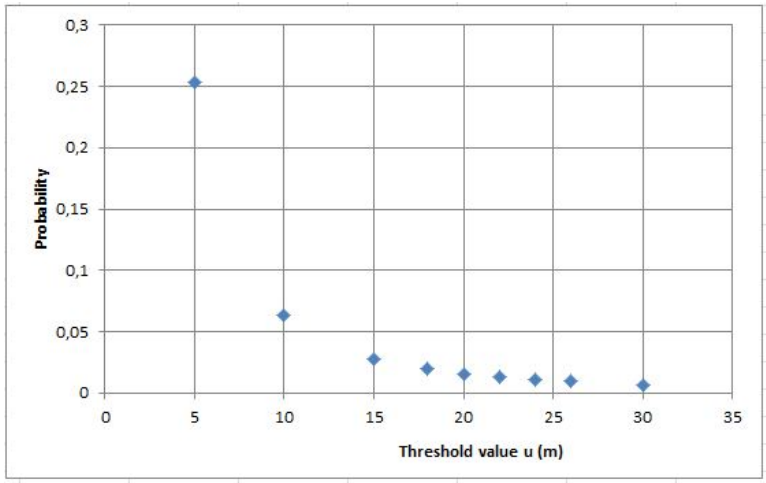

Figure 7.2: The probability of exceedance of specific threshold values calculated through Chebyshev's inequality theorem. The probability decreases with increasing threshold values.

7.2 Generalized Pareto distribution and Exponential distribution

The sensitivity of the shape parameter from the generalized Pareto distribution can be tested by varying the threshold value (Ekeberg et al., 2013b). The parameters in the Generalized Pareto distribution were estimated with a 95% confidence interval. The shape parameter was found to decrease slightly with increasing threshold value, with a trend towards 0. All values for the shape parameter was with 95% confidence within 0–0.28. The shape parameter estimates with 95% confidence interval are shown in **Fig. 7.3**.

Figure **7.4** shows the Generalized Pareto distribution of the keel draft data. Figure **7.5** shows the comparison between the Generalized Pareto distribution and a calculated cumulative distribution of the actual measurements.

With a shape parameter equal to 0, the Generalized Pareto distribution becomes the Exponential distribution with parameter $1/\tilde{\sigma}$. The exponential distribution was then calculated using equation (6.44) and is shown in **Fig. 7.6**. This distribution was compared to the Generalized Pareto distribution as well as the cumulative distribution of the data in figure **7.7**.

Equations (6.55) and (6.56) was used in calculating the 100-year return level for both the Generalized Pareto distribution **Fig. 7.8**, and the exponential distribution **Fig. 7.9**. The

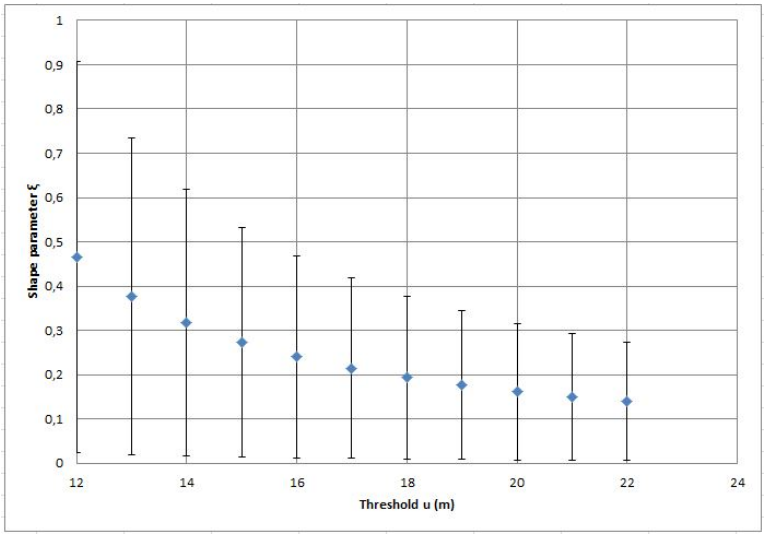

Figure 7.3: The estimates shape parameter ξ as a function of threshold value u with 95% confidence intervals.

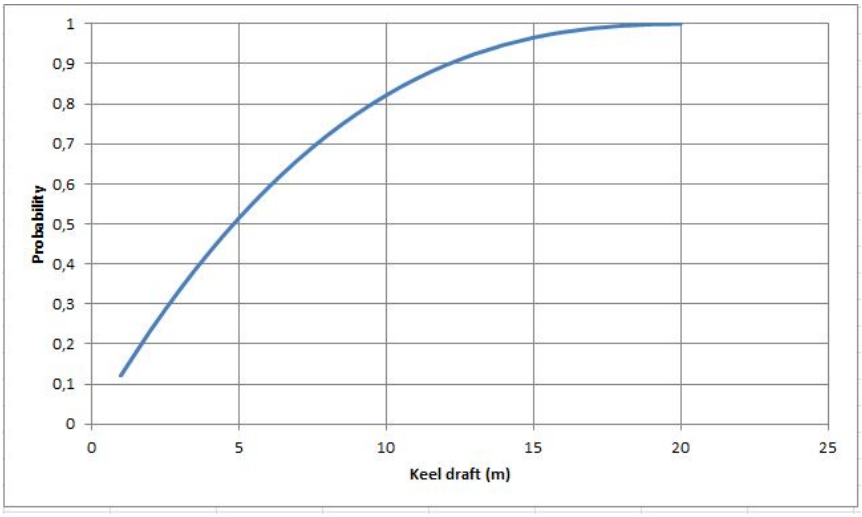

Figure 7.4: The estimated Generalized Pareto distribution of the keel draft data.

Generalized Pareto distribution gives an increase in return level with increasing threshold value. The exponential distribution gives a slight decrease in return level as the threshold value increases, but appears to stabilize at around 40 m. A comparison of the two 100-year return values are shown in **Fig. 7.10** with the 95% confidence intervals included. The two deviates up to an approximate threshold value of 15 m, before the confidence intervals overlap. From a threshold value of 15 m, the data gave a 100-year return value between

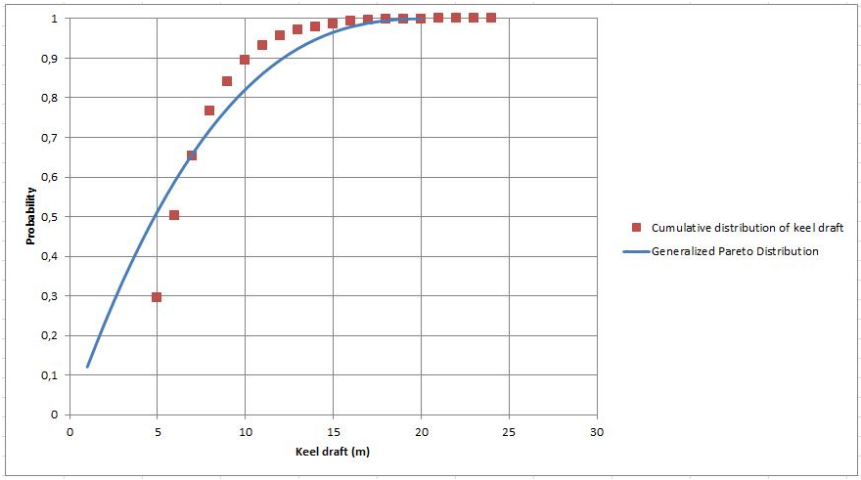

Figure 7.5: The estimated Generalized Pareto distribution of keel draft data plotted vs the calculated cumulative distribution of the measured keel draft.

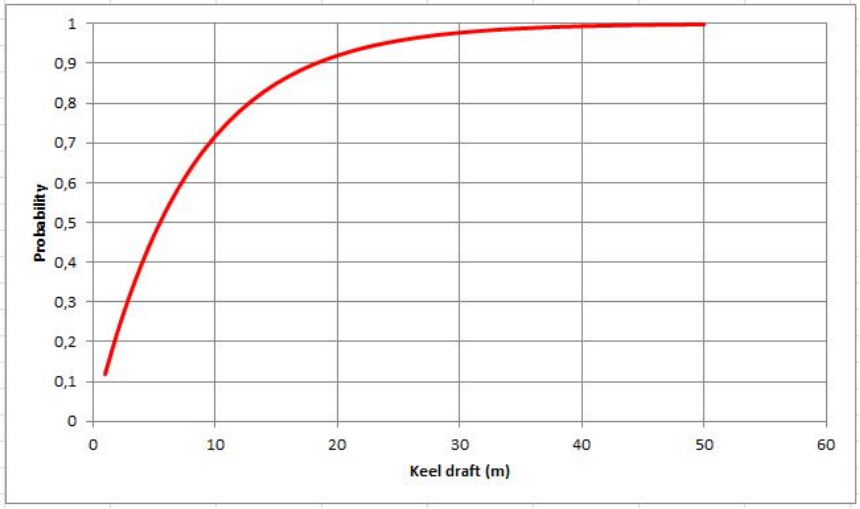

Figure 7.6: The estimated Exponential distribution of the keel draft data.

37 and 45 m.

7.3 Weibull distribution

The ridge keel draft data was analyzed using a three-parameter Weibull distribution. The observations are counted in number of keels within intervals of 0.1 m, from the minimum

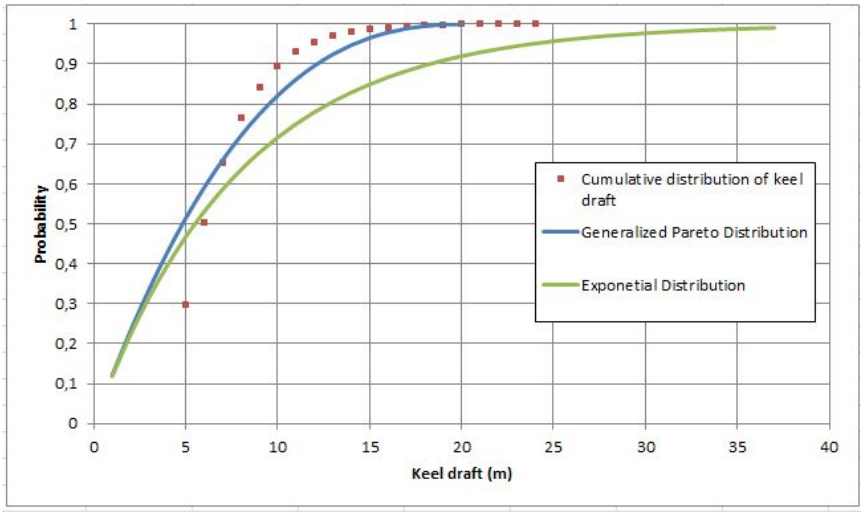

Figure 7.7: The estimated Generalized Pareto distribution and the estimated Exponential distribution vs the calculated cumulative distribution.

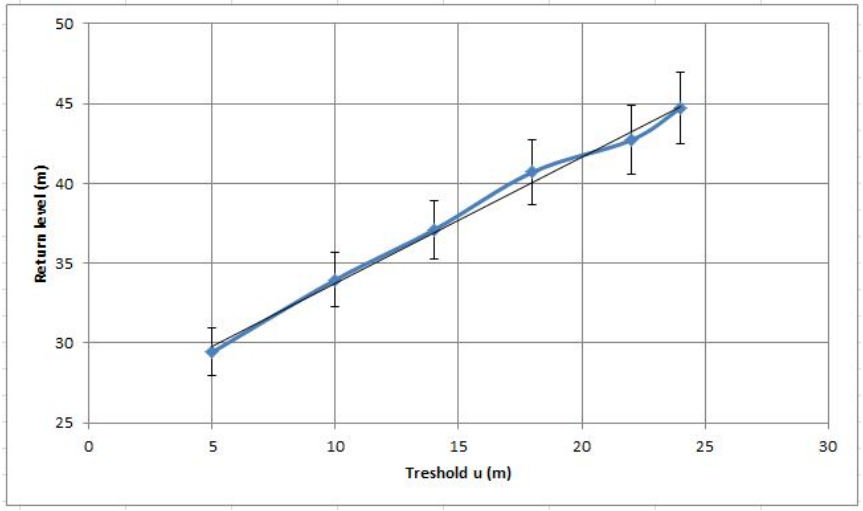

Figure 7.8: The estimated 100-year return level for varying threshold values for the Generalized Pareto distribution.

draft value of 5 m till the highest observed draft of 24.967 m. The adjacent cumulative probabilities were plotted, as seen in figure **7.11**.

To find the extreme values from this distribution, the cumulative distribution can be linearized by taking the double natural logarithm. This can then be expressed as a straight line function $y = ax + b$. Here, y represents the double natural logarithm of the probability

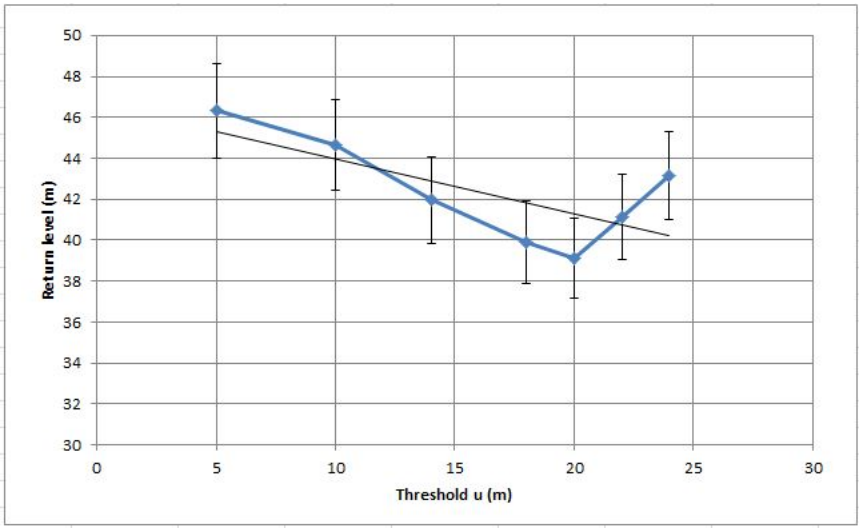

Figure 7.9: The estimated100-year return level for varying threshold values for the Exponential distribution.

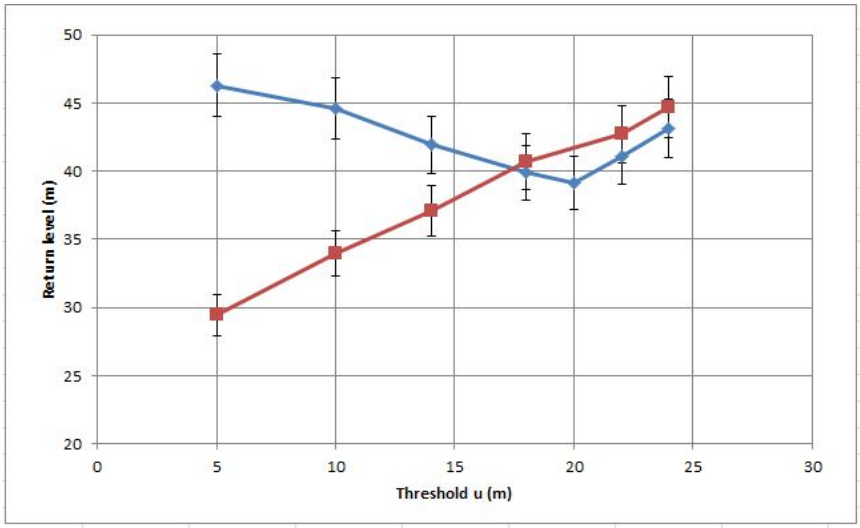

Figure 7.10: The estimated 100-year return level for varying threshold with 95% confidence interval, for both the Generalized Pareto distribution and the Exponential distribution.

of exceedance per year, Ph_{k}, a is the shape parameter β, and x the natural logarithm of $x - \lambda$, with λ being the location parameter. The location parameter was chosen to be the threshold value 2.5 m.

Figure **7.12** shows the results after the first linearization. A trend-line is introduced

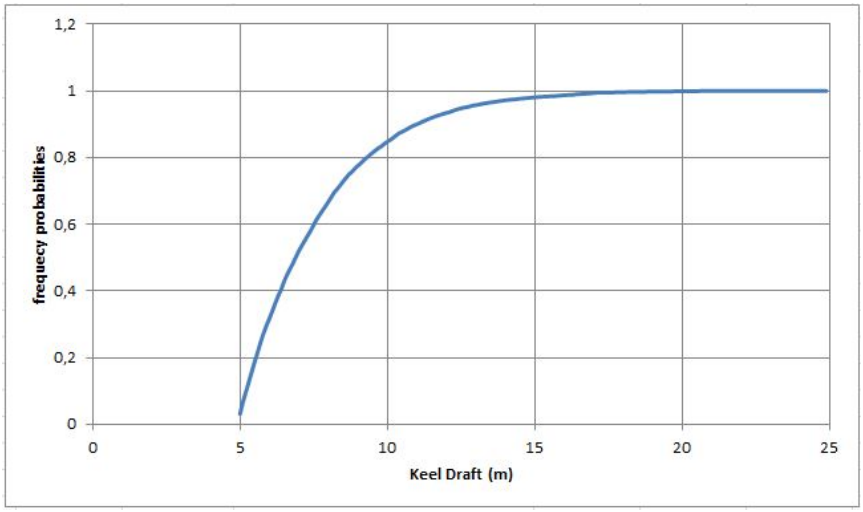

Figure 7.11: The cumulative probability distribution of the three-parameter Weibull distribution.

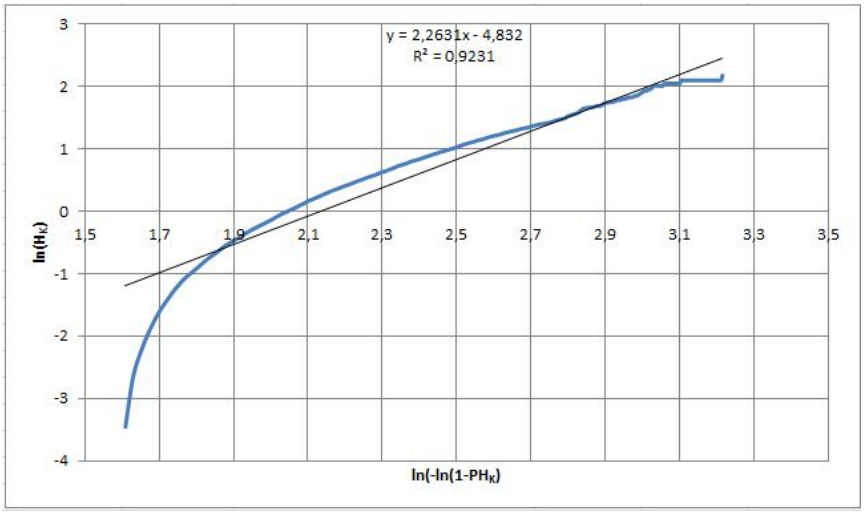

Figure 7.12: The results after taking the natural logarithm of the cumulative probability distribution of the three-parameter Weibull distribution.

with an associated correlation coefficient of $R^2 = 0.9231$, and a straight line function y. The natural logarithm is introduces a second time to improve the linearization. Figure **7.13** shows the results. Here the correlation coefficient is higher, meaning a higher correlation with $R^2 = 0.9944$. The straight line function : $y = 1.4228x$–2.1951.

To calculate the return level for a 100-year return period, equation (6.37) was used to find the exceedance probability per year. The straight line function was used and solved

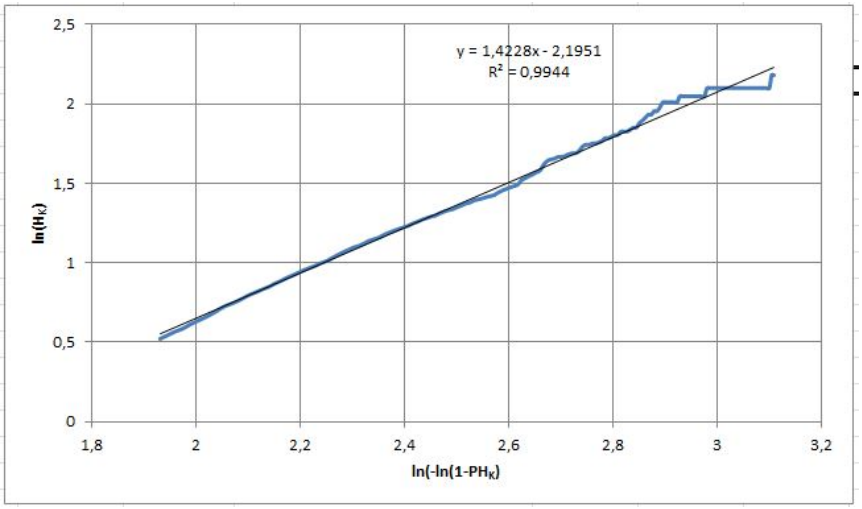

Figure 7.13: The results after taking the natural logarithm of the cumulative probability distribution of the three-parameter Weibull distribution a second time, giving a more linearized result.

for x, giving the natural logarithm of $x - \lambda$. From this the return level was calculated to be 29.065 m for a 100-year return period.

Chapter 8

Discussion

Ekeberg et al. (2013d) found the mean value of ice ridge keel draft in the season 2006/2007 to be 7.52 m. The present study found the mean value to be 7.7085 m, which is 0.265 m higher than that found by Ekeberg et al. (2013d). The median for the keel draft data was 0.235 m higher in this study than in Ekeberg et al. (2013d). The slightly higher results from this study compared to that of Ekeberg et al. (2013d) is difficult to give an exact reason for, as the same threshold value at 2.5 m and the same minimum draft value at 5 m was used in both studies. Small differences in methodology and computer coding may cause this slight difference.

Ekeberg et al. (2012) found by analyzing the same data from the moored IPS instrument in the Fram Strait in the season 2006/2007, that between 2 and 7 ice ridges deeper than 15 m passed by the instrument every day. Ekeberg et al. (2012) concluded that a total of 4 ridges deeper than 30 m were observed in 2006/2007. According to the analysis performed by Ekeberg et al. (2012) of the season 2006/2007 in the Fram Strait, the mean keel draft was 7.5 m, the median draft 6.7 m and a maximum draft of 34.5 m. The maximum draft found in this study was 24.976 m, a much lower result than Ekeberg et al. (2012).

Ekeberg et al. (2013d) found that the number of ridges and the mean keel draft decreased from 2006-2011. By excluding data from the season of 2006/2007 (which had a high number of observed ridges), the total decrease in numbers was 408 ridges per year. Ekeberg et al. (2013d) concluded that the decrease in mean and median keel draft of the entire period from 2006-2011, was approximately 13 cm per year. According to Ekeberg et al. (2013d), the probability of observing a deep ridge has decreased with every season since the start of observation in 2006. Ekeberg et al. (2013d) found a clear seasonality of the ice concentration, with a concentration of 90% in the winter months (October – April), and a decrease from May until peak low in July – August with 10–70% ice concentration.A similar study in decreasing (or eventual increasing) in the number of ice ridges, was not possible in the present study, as the data used was measurements from only one season.

8.1 Smoothing of data and ice ridge keel area

The smoothed data set resulted in a slightly higher mean keel draft value as well as a decrease in the maximum keel draft value. The smoothing effect of a data set was studied by Ekeberg et al. (2013a). Ekeberg et al. (2013a) concluded that this effect, the decrease in maximum value contrasted the increase in mean value, followed by merging of ice ridges due to the smoothing method applied. With a running average potential measurement errors is reduced, and the through between two ice ridges are increased (Ekeberg et al., 2013a). As this space increases, the probability of adjacent ridges being defined as one increases, and the width of the now defined one ridge, increases. An estimate from Ekeberg et al. (2012) suggests that there are a $3-4$ times higher frequency of ice ridges in the Fram Strait compared with the Beaufort Sea.

There is a correlation between area of the ice ridge keel and the ice ridge keel width, as seen in figure **7.1**. The large outliers in this graph may be anomalies and could possibly be excluded from further analysis. The width and the area are both dependent of threshold value; Ekeberg et al. (2013c) found that an increase in the threshold value of 0.5 m (from 2.5 to 3 m), led to an increase in mean keel width and mean keel area of 12%. This increase may also be caused by the same reason as the increase of the mean keel draft value.

8.2 Chebyshev's inequality

The probability of encountering an ice ridge with a certain depth is shown in **Table. 7.1**. Ekeberg et al. (2012) found that the probability of ice ridges deeper than 20 m in the Fram Strait varied between 0.03% and 0.2%. This is consistent with the result in **Table. 7.1**, with a probability of an ice ridge deeper than 20 m of 0.15%. Pilkington and Wright (1991) found the same probability in the Beaufort Sea to be 0.01%, which corresponds with there being observed more ridges in the Fram Strait (Ekeberg et al., 2012). However, the low value found by Pilkington and Wright (1991) could be explained by the low minimum draft value chosen (3 m) as opposed to 5 m in the present study and in Ekeberg et al. (2012), and the value could hence be higher with a higher choice of minimum draft value (Ekeberg et al., 2012).

Ekeberg et al. (2013b) analyzed the extreme ice ridge keel drafts in the Fram Strait from 2006 – 2011 and found more ice ridges in the season of 2006/2007 than in any other season, and with this, a higher probability of encountering larger ice ridges.

8.3 Extreme values

The choosing of a draft threshold to filter eventual maximum keel draft values that does not lie within the extreme of the maximum draft distribution, is a sensitive task, as the ridge keel population decreases rapidly with increasing keel draft threshold (Ross et al.,

2012). The ideal threshold value is one that is at or near the extreme of the distribution tail, while also giving a significant population size (Ross et al., 2012).

By increasing the threshold value the number of observations is reduced, but this measure should also decrease an eventual bias that can occur. The increase in threshold also increases the chances of getting independent observations. Ekeberg et al. (2013b) compared results from different threshold values, and found that the results varied little, giving support to the theory about independent observations.

Figure **7.5** shows a comparison between the estimated Generalized Pareto distribution and the calculated cumulative distribution of the ice ridge keel draft data. For the Generalized Pareto distribution to be considered a valid estimate, it is expected that it will follow the cumulative distribution curve in a plotted graph, as is evident in figure **7.5**. Figure **7.7** shows the same comparison with the cumulative distribution, with the Exponential distribution included. All three curves follow each other relatively well, which can be interpreted as the Generalized Pareto distribution and the Exponential distribution being considered good estimates for the ice ridge keel draft.

The Generalized Pareto distribution is reduced to the exponential distribution when the shape parameter is equal to 0. In addition to this, the three-parameter Weibull distribution is reduced to the Exponential distribution when its shape parameter is equal to 1. This means that all tree distributions are correlated to a certain degree, and the distributions should have a similar graph shape according to the cumulative probability distribution. All distributions were approximated with the log-likelihood method from equation (6.11) and fitted into figure **8.1**.

8.4 100-year return level

The 100-year return level calculated from the Generalized Pareto distribution and the Exponential distribution was very similar, with values ranging from $37 - 45$ m. The three-parameter Weibull distribution gave a lower result of 29 m. The shape parameter in the three-parameter Weibull distribution was estimated to be 1.4228, a higher result than 1.0, which would reduce the distribution to the Exponential distribution. This high result in shape parameter is a possible reason to why the 100-year return value was so low for the three-parameter Weibull distribution compared to the Generalized Pareto distribution and the Exponential distribution.

Ross et al. (2012) gave a prediction on the 100-year return values in the Fram Strait, using data from measurements obtained in the season of 2008/2009. The result here was 33 ± 4 m. Ekeberg et al. (2013b) found the 100-year return value in the Fram Strait using data from 2006-2011, to lie in the range of $37 - 41$ m. The results from Ross et al. (2012) are lower compared to the results from Ekeberg et al. (2013b) and compared to the results from the present study. Ekeberg et al. (2013b) concluded with the results from Ross et al. (2012) being too low, since they found ice ridge keels of size greater than 33 m. Assuming

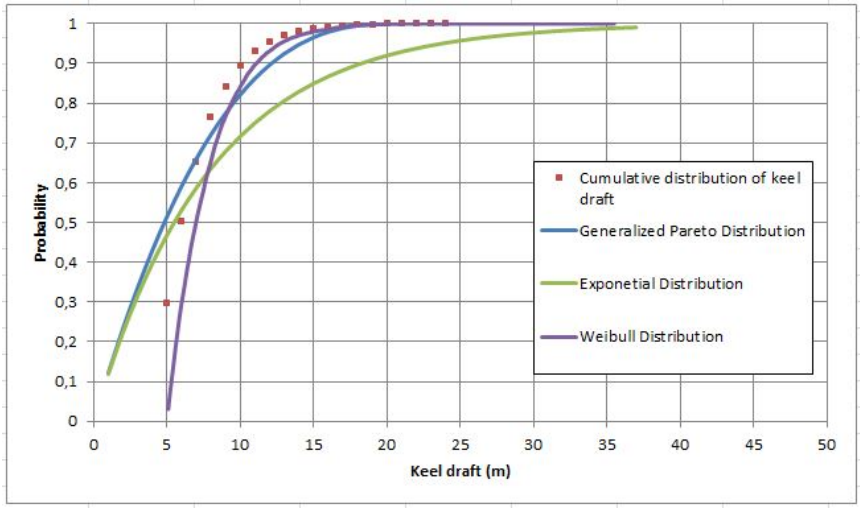

Figure 8.1: The estimated Generalized Pareto distribution, the estimated Exponential distribution and the estimated Weibull distribution of the ice ridge keel draft data vs the calculated cumulative distribution.

this is correct, the estimated 100-year return values from the Generalized Pareto distribution and the Exponential distribution in this study, corresponds well with previous results.

The 100-year return value in the Beaufort Sea was by Ross et al. (2012) estimated to be 32 ± 2 m, while Wadhams (2012) found the same to be in the range of 30–35 m. The results of 100-year return value from the Beaufort Sea are then lower than the results from the Fram Strait, as expected, as there are more ice ridges observed in the Fram Strait. Wadhams (2012) analyzed keel drafts in the Beaufort Sea and concluded that while the Beaufort Sea coastal zones are dominated by first-year ice, ridges cannot be expected to form beyond 45 m water depth. Wadhams (2012) compared the results of this study with a similar analysis done with data collected from the same area in 1976. The mean draft of the ice cover was reduced from 3.81 m in 1976 to 2.58 m in 2007. The 1000-year return period estimated from both periods showed that this value had decreased from 55 m in 1976 to 39 m in 2007. Wadhams (2012) concluded that the predictions for maximum keel depths were substantially reduced from 1976 to 2007, and hence that eventual scouring of ridge keels occurs at significantly shallower waters.

8.5 Ice ridge observations

Young ice is thinner and weaker than old ice (Wadhams, 2000). With a higher frequency of young ice, more deformed ice, despite of the same external forces and ice concentration, is possible (Ekeberg et al., 2013d). An ice floe will continuously move, break up and refreeze, causing redistribution of the ice within, and could in combination with younger ice,

cause an increase in the number of old ice ridges, even though no new ridges are formed (Ekeberg et al., 2013d). This redistribution of the ridge itself could cause ULS instrumentation false observations of increased ridge numbers. Within old ice, there has been enough time for leads to open; a fracture through the ice caused by wind or ocean currents, big enough to be navigable by surface vessels (Leppäranta, 2011). These open fractures can cause more ridges to be made. Young ice is likely to contain fewer ice ridges, less consolidated and hence smaller ice ridges than old ice (Hansen et al., 2013). These young ice ridges have therefore a higher tendency for disintegration than old ice ridges, which could further lead to accelerated decrease in mean ice thickness in the Arctic (Hansen et al., 2013).

The older the ice ridge is, the more time it has to grow. It can therefore be postulated that multi-year ice ridges have keel drafts larger than first-year ice ridges. However, the Upward Looking Sonar instruments do not distinguish between ice features. And some of the assumed ice ridges may be ice bergs drifting alongside the ice ridges. Ice bergs are not made by thermodynamically, rubbled, and consolidated ice, but are broken off, freshwater pieces from glaciers, that are formed from accumulation of snow. These features are not possible to distinguish from ice ridges in data collected from ULS instruments. However, ice bergs are often very large ice features, larger than the largest observed ice ridge. Because of this, if an ice feature in ice ridge keel analysis has a very high draft value compared to estimated return values, it is discarded as an ice berg.

Ekeberg et al. (2013d) postulated that the observed reduction in the number of ridges and its draft value coincides with observed reduction in fraction of ice thicker than 5 m (Hansen et al., 2013). This decrease in ice thicker than 5 m, Ekeberg et al. (2013d) hypothesized must be related to change in the ridge population, and will be observed as fewer ridges, smaller ridges or as a change in the ridge geometry.

Ekeberg et al. (2013d) made a list of possible causes for the changes in ridge population:

- Drift speed
- Current and wind
- Ice cover strength
- Shape of the ice ridge keels
- Ice concentration
- Origin of ice
- Ice age
- Melting

Ekeberg et al. (2013d) concluded with the reduced age of the ice cover being the most likely cause for the observed reduction in mean keel draft and the number of ridges.

8.6 Ice thickness observations

The ice in the Fram Strait is a mixture of old ice and first-year ice, most of it originating from the Laptev Sea and the East Siberian Sea (Hansen et al., 2013). The ice thickness in the Fram Strait is very dynamic, and no unique level exists (Ekeberg et al., 2012). According to Maslanik et al. (2011) the amount of multi-year ice in the Arctic has decreased and become younger. The extent of multi-year ice during March has declined by 33% from 1980 to 2011, and during September by 50%. The fraction of the total ice extent, first-year and multi-year ice, made up of multi-year ice in the Arctic Ocean decreased from 75% to 45% in the mid 1980 to 2011 respectively Maslanik et al. (2011). According to Haas et al. (2010), the areal extent of summer sea ice in the Arctic has decreased at a rate of 11.2% per decade over the last 30 years. Even though it has a declining trend, it must be taken into consideration that sea ice is subject to large regional and inter-annual variations (Haas et al., 2010).

The thinning and decreasing of the ice cover in the Arctic are expected to continue resulting from climate change, amplified by the ice-albedo feedback (Haas et al., 2010). Ice thickness distribution in the Arctic Ocean typically features a long tail and two modal peaks, where the lower modes represent level first-year ice and the upper modes level old ice (Haas et al., 2010). This display of the most frequent occurring ice thicknesses in the Arctic reflects thermodynamic processes (Hansen et al., 2013). Temporal changes in the old-ice thickness modes display changes in the climatic factors that control seasonal growth, melt and age of the ice cover (Hansen et al., 2013). The width of the modal peak can provide an estimate of the age of the ice; old ice has experienced several seasons of freezing and melting, and is therefore more likely to produce wider modal peaks than younger ice (Hansen et al., 2013). The thermodynamically grown ice is encircled by dynamically deformed ice (Hansen et al., 2013).

According to Hansen et al. (2013) there was a decrease in ice age from 2005 – 2008 in the Fram Strait, followed by an increase in age until 2011 (when the observation period ended). Hansen et al. (2013) found a mean ice thickness in the Fram Strait in 2006 of 3.3 m and in 2007 3.0 m. The amount of ridged ice above 5 m decreased to 5% in 2011 (Hansen et al., 2013).(Hansen et al., 2013) found no sign of recovery of mean ice thickness and ice thicker than 5 m in observations from 2008 – 2011. The age of the ice cover, as well as thermodynamic growth and melt of sea ice, is all affected by parameters such as snow thickness, long- and shortwave radiation, air temperature and ocean heat flux (Hansen). Wind force, ice thickness and availability of thin ice sheets for deformation, and the capacity of the ice pack to transfer stress and pressure for formation are important factors in the growth and decay of ridged ice (Amundrud et al., 2004). Changes in any of the factors above, could affect the relative number of ridges in an ice pack, as well as the thickness and age of the ice. Even small changes in the ocean heat flux would influence

the ice thickness and the fraction of ridged ice (Hansen et al., 2013). Amundrud et al. (2004) found through observation that ridged ice has a more rapid rate of melting than the surrounding level ice. The ocean heat melt the consolidated layer and the bonds between ice blocks in the ridge keel brake, causing the ridge to disintegrate.

The ice in the Arctic are in constant movement, meaning the observed ice thickness distribution is a product of several processes, featuring both temporal and spatial variability (Hansen et al., 2013). The Fram Strait includes ice originating from several locations in the Arctic Ocean, and the thickness observed here is the sum of the time varying thermodynamic and dynamic processes acting on the ice, from its origin to the Fram Strait. Hansen et al. (2013) assumed the loss of ridged ice has occurred due to solar heating and ice-albedo feedback, as well as possible increase in the ocean heat flux. Parkinson and Comiso (2013) found that the Arctic sea ice cover reached its lowest value at end of summer 2012 in 112 years.

Chapter 9

Conclusion

The present thesis studied sea ice ridge morphology and applied extreme value analysis to estimate the 100-year return value for ice ridge keel draft and finding the probability of extreme values of these in the Fram Strait, by using data collected from Upward Looking sensors deployed in the season of 2006/2007 at 79° N. Three methods was employed; the Generalized Pareto distribution, the Exponential distribution and the three-parameter Weibull distribution.

The Generalized Pareto distribution was simplified to the Exponential distribution due to the shape parameter value being close to 0. The result was a 100-year return value of ice ridge keel drafts in the range of 37–45 m. The three-parameter Weibull distribution gave a lower 100-year return level of 29 m. The results from the Generalized Pareto method and the Exponential method was compared to previous studies, and found to be equal to or somewhat higher than previous studies. It was also found to be higher than corresponding estimates of ice ridge keel drafts in the Beaufort Sea. The mean ice ridge keel draft value was found to be 7.7 m. The shallowest ice ridge keel observed had a draft of 5.0 m, while the deepest ice ridge keel was 24.97 m deep. The mean keel width was found to be 63.05 m, with a minimum value of 6.35 m and a maximum value of 1969.3 m.

The fraction of ice observed defined as ice ridges was 0.0299, approximately 3%. Chebyshev's inequality was used to find the estimated probability of encountering ridges with keel drafts larger than 20 m. The result was 0.15%, and compared to previous studies in the Fram Strait with results spanning from 0.03% to 0.2%, this was found to be satisfying.

The limited data used in this thesis needs to be considered in evaluating the results. A large data set with a long time set should be used in any extreme value analysis to get the best estimates.

Bibliography

, 2014. Ice Profiler Model IPS5 Specifications. ASL Environmental Sciences Inc.

Amundrud, T. L., Melling, H., Ingram, R. G., 2004. Geometrical constraints on the evolution of ridged sea ice. Journal of Geophysical Research 109, CO6005.

Bertsekas, D. P., Tsitsiklis, J. N., 2002. Introduction to Probability, 2nd Edition. Athena Scientific.

Castillo, E., Hadi, A. S., Balakrishnan, N., Sarabia, J. M., 2005. Extreme Value and Related Models with Applications in Engineering and Science. John Wiley and Sons Inc.

Coles, S., 2001. An Introduction to Statistical Modeling of Extreme Values. Springer.

Dougherty, E. R., 1990. Probability and Statistics for the Engineering, Computing and Physical Sciences. Prentice-Hall Inc.

Ekeberg, O.-C., Høyland, K., Hansen, E., 2012. Ice ridge identification methods and analysis of upward looking sonar data from fram strait 2006-2011. Ice Research for a Sustainable Environment, 21st IAHR International Symposium on Ice, Dalian, China.

Ekeberg, O.-C., Høyland, K., Hansen, E., 2013a. Converting a time series of ice draft data from an upward looking sonar to equidistant ice draft data- effects on keel characteristics.

Ekeberg, O.-C., Høyland, K., Hansen, E., 2013b. Extreme keel drafts in the fram strait 2006-2011. 22nd International Conference on Port and Ocean Engineering under Arctic Conditions, Espoo, Finland.

Ekeberg, O.-C., Høyland, K., Hansen, E., 2013c. Ice ridge keel geometry and shape derived from one year of upward looking sonar data in the fram strait. Preprint submitted to Cold Regions Science and Technology.

Ekeberg, O.-C., Høyland, K., Hansen, E., 2013d. Reduction in the number and thickness of ridges in the transpolar drift in the fram strait during 2006-2011-draft. Geophysical Research Letters.

Fissel, D. B., Marko, J. R., Melling, H., 2004. Upward looking ice profiler sonar instruments for ice thickness and topography measurements. ASL Environmental Sciences Inc., Presented at Oceans '04 MTS/IEEE/ Techno-Oceans '04, Kobe, Japan.

Haas, C., Hendricks, S., Eicken, H., Herber, A., 2010. Synoptic airborne thickness surveys reveal state of arctic sea ice cover. Geophysical Research Letters 37, 1–5.

Hagen, P. C., 2010. Innføring i Sannsynlighetsregning og Statistikk, 6th Edition. Cappelen Damm AS.

Hansen, E., Gerland, S., Granskog, M. A., Pavlova, O., Renner, A. H. H., Haapala, J., Løyning, T. B., Tschudi, M., 2013. Thinning of arctic sea ice observed in fram strait: 1990-2011. Journal of Geophysical Research: Oceans 118, 5202–5221.

Harder, M., Lemke, P., Hilmer, M., 1998. Simulation of sea ice transport through fram strait: Natural variability and sensitivity to forcing. Journal of Geophysical Research 103, 5595–5606.

Heinonen, J., 2004. Constitutive modeling of ice rubble in first-year ridge keel. Ph.D. thesis, Helsinki University of Technology.

Hopkins, M. A., 1998. Four stages of pressure ridging. Journal of Geophysical Research 103, 21883–21891.

Høyland, K., 2012. Lecture in tba4265 marine physical environment, ntnu.

Jewett, J. W., Serway, R. A., 2008. Physics for Scientists and Engineers, seventh edition Edition. Thomson Brooks/Cole.

Kotz, S., Nadarajah, S., 2000. Extreme Value Distributions Theory and Applications. Imperial College Press.

Kwok, R., Cunningham, G. F., Pang, S. S., 2004. Fram strait sea ice outflow. Journal of Geophysical Research 109, 1–14.

Leppäranta, M., 2011. The Drift of Sea Ice, 2nd Edition. Springer.

Leppäranta, M., Lensu, M., Kosloff, P., Veitch, B., 1995. The life story of a first-year sea ice ridge. Cold Region Science and Technology 23, 279–290.

Marchenko, A., 2013. Lecture in structure and physical properties of sea ice, at-211 ice mechanics, loads on structures and instrumentation, unis.

Maslanik, J., Stroeve, J., Fowler, C., Emery, W., 2011. Distribution and trends in arctic sea ice age through spring 2011. Geophysical Research Letters 38, 1–6.

Melling, H., Johnston, P. H., Riedel, D. A., 1995. Measurements of the underside topography of sea ice by moored subsea sonar. Journal of Atmospheric and Oceanic Technology 12, 589–602.

Notz, D., 2013. Lecture in agf-211 air-ice-sea interaction i, unis.

Obert, K. M., Brown, T. G., 2011. Ice ridge keel characteristics and distribution in the northumberland strait. Cold Regions Science and Technology 66, 53–64.

Parkinson, C. L., Comiso, J. C., 2013. On the 2012 record low arctic sea ice cover: Combined impact of preconditioning and an august storm. Geophysical Research Letters 40, 1356–1361.

Pilkington, C. R., Wright, B. D., 1991. Beaufort sea ice thickness measurements from an acoustic, under ice, upward looking ice keel profiler. The International Society of Offshore and Polar Engineers, First International Offshore and Polar Engineering Conference, Edinburgh, United Kingdom.

Ross, E., Fissel, D., Marko, J., Reitsma, J., 2012. An improved method of extremal value analysis of arctic sea ice thickness derived from upward looking sonar ice data. Offshore Technology Conference, Houston, Texas, USA, Arctic Technology Conference.

Ross, S. M., 2009. Introduction to Probability and Statistics for Engineers and Scientists, 4th Edition. Elsevier Academic Press.

Timco, G. W., Burden, R. P., 1997. An analysis of the shapes of sea ice ridges. Cold Region Science and Technology 25, 65–77.

Tucker, W. B., Govoni, J. W., 1981. Morphological investigations of first-year sea ice pressure ridge sails. Cold Region Science and Technology 5, 1–12.

Vinje, T., Nordlund, N., Ånund Kvambekk, 1998. Monitoring ice thickness in fram strait. Journal of Geophysical Research 103, 10,437–10,449.

Wadhams, P., 1983. The prediction of extreme keel depths from sea ice profilers. Cold Regions Science and Technology 6, 257–266.

Wadhams, P., 2000. Ice in the ocean. Gordon and Breach Science Publisher.

Wadhams, P., 2012. New predictions of extreme keel depths and scour frequencies for the beaufort sea using ice thickness statistics. Cold Region Science and Technology 76-77, 77–82.

Wadhams, P., Horne, R. J., 1980. An analysis of ice profiles obtained by submarine sonar in the beaufort sea. Journal of Glaciology 25, 401–424.

Werner, K., Frank, M., Teschner, C., Muller, J., 2013. Neoglacial change in deep water exchange and increase of sea-ice transport through eastern fram strait: evidence from radiogenic isotopes. Quaternary Science Reviews, 1–18.

Sources of Errors

The data used for calculations in this thesis, and the methods for calculations, was lost for a period of time for the author, due to technical problems and an uncooperative computer. This caused the author having to do all calculations a second time very late in the process.

Due to technical difficulties with the data, time data for the observation values was unavailable. This limited the analysis somewhat, but the extreme values and subsequent return periods were found independently of the time data. However, a graphical visualization of a single ice ridge keel was unfortunately not possible to complete without these data.

Rundoff errors are a possibility in computer calculation and estimation, which is inexact computer floating point arithmetic. These occur in several floating point operations, and may cause different results in analyzing the same data, but in different computer programs or on different computers.

Several computations performed in this thesis is estimations, which are not exact calculations. In using estimates further in calculations, these uncertainties continue through the calculations, and propagate through computations, giving rise to according errors.

To find and analyze every single ice ridge in the Fram Strait, the local level ice thickness has to be found for all observations. More data should be used in analysis such as those performed in this thesis. Data collected over one year gives a large enough data set to get approximate estimates and results. However, a larger data set collected over several years, will give better estimations and results, and a possibility for comparison between years and analyze an eventual trend in the data.